Article

Validation and Conformity Testing of Sentinel-3 Green Instantaneous FAPAR and Canopy Chlorophyll Content Products

Fernando Camacho [1,*], Enrique Martínez-Sánchez [1], Luke A. Brown [2,3], Harry Morris [3,4], Rosalinda Morrone [4,5], Owen Williams [3], Jadunandan Dash [3], Niall Origo [4], Jorge Sánchez-Zapero [1] and Valentina Boccia [6]

[1] Earth Observation Laboratory (EOLAB), 46980 Paterna, Spain; enrique.martinez@eolab.es (E.M.-S.); jorge.sanchez@eolab.es (J.S.-Z.)

[2] School of Science, Engineering & Environment, University of Salford, Manchester M5 4WT, UK; l.a.brown4@salford.ac.uk

[3] School of Geography and Environmental Science, University of Southampton, Highfield, Southampton SO17 1BJ, UK; harry.morris@npl.co.uk (H.M.); owenw2203@gmail.com (O.W.); j.dash@soton.ac.uk (J.D.)

[4] Climate and Earth Observation Group, National Physical Laboratory, Teddington, Middlesex TW11 0LW, UK; rosalinda.morrone@downforce.tech (R.M.); niall.origo@npl.co.uk (N.O.)

[5] Downforce Technologies, Botley, Oxford OX2 0JB, UK

[6] European Space Research Institute, European Space Agency, 00044 Frascati, Italy; valentina.boccia@esa.int

* Correspondence: fernando.camacho@eolab.es

Abstract: This article presents validation and conformity testing of the Sentinel-3 Ocean Land Colour Instrument (OLCI) green instantaneous fraction of absorbed photosynthetically active radiation (FAPAR) and OLCI terrestrial chlorophyll index (OTCI) canopy chlorophyll content (CCC) products with fiducial reference measurements (FRM) collected in 2018 and 2021 over two sites (Las Tiesas—Barrax, Spain, and Wytham Woods, UK) in the context of the European Space Agency (ESA) Fiducial Reference Measurement for Vegetation (FRM4Veg) initiative. Following metrological principles, an end-to-end uncertainty evaluation framework developed in the project is used to account for the uncertainty of reference data based on a two-stage validation approach. The process involves quantifying uncertainties at the elementary sampling unit (ESU) level and incorporating these uncertainties in the upscaling procedures using orthogonal distance regression (ODR) between FRM and vegetation indices derived from Sentinel-2 data. Uncertainties in the Sentinel-2 data are also accounted for. FRM-based high spatial resolution reference maps and their uncertainties were aggregated to OLCI's native spatial resolution using its apparent point spread function (PSF). The Sentinel-3 mission requirements, which give an uncertainty of 5% (goal) and 10% (threshold), were considered for conformity testing. GIFAPAR validation results revealed correlations > 0.95, RMSD ~0.1, and a slight negative bias (~−0.06) for both sites. This bias could be partly explained by the differences in the FAPAR definitions between the satellite product and the FRM-based reference. For the OTCI-based CCC, leave-one-out cross-validation demonstrated correlations > 0.8 and RMSDcv ~0.28 g·m^{-2}. Despite the encouraging validation results, conclusive conformity with the strict mission requirements was low, with most cases providing inconclusive results (driven by large uncertainties in the satellite products as well as by the uncertainties in the upscaling approach). It is recommended that mission requirements for bio-geophysical products are reviewed, at least at the threshold level. It is also suggested that the large uncertainties associated with the two-stage validation approach may be avoided by directly comparing with spatially representative FRM.

Keywords: fiducial reference measurements; OLCI; uncertainty; upscaling; conformity testing

1. Introduction

Earth observation (EO) satellite sensors provide a unique way to monitor essential climate variables and surface properties over the globe that are required to understand our

climate and Earth system processes [1]. The need for post-launch calibration and validation (Cal/Val) of satellite sensors and derived products is well-established [2–4]. While post-launch calibration against independent reference data ensures that unforeseen changes are accounted for, validation is essential to deliver satellite-derived products to users assessing, in an independent way, their uncertainties and confirming the expected performance of a mission [5]. The conformity testing process determines if the estimated quantity falls within the range of tolerable values (i.e., mission/user requirements) or not [6].

The Quality Assurance Framework for Earth Observation (QA4EO) guidelines state that EO data and derived products should be provided with an indicator of quality traceable to reference standards (preferably SI) so that users can assess suitability for their application (i.e., their fitness for purpose) [7]. A key element of QA4EO relates to validation through independent reference data. Consequently, the reference data must also be characterised following QA4EO principles [5]. The need to evidence these principles for Cal/Val was the basis for the term 'Fiducial Reference Measurement (FRM)'. FRMs are 'a suite of independent, fully characterised, and traceable (to a community agreed reference, ideally SI) measurements of a satellite relevant measurand, tailored specifically to address the calibration/validation needs of a class of satellite-borne sensor and that follow the guidelines outlined by the QA4EO' [5].

Within the ESA FRM programme, the Fiducial Reference Measurements for Vegetation (FRM4Veg) (http://www.frmveg.org/, accessed on 18 July 2024) initiative aims, for the first time, to apply metrological principles to the validation and conformity testing of vegetation bio-geophysical products initially derived from Copernicus Sentinel-2, Sentinel-3, and PROBA-V missions [8]. An end-to-end evaluation framework has been established for surface reflectance [9], for the fraction of absorbed photosynthetically active radiation (FAPAR), and for canopy chlorophyll content (CCC) [10]. For FAPAR and CCC, the process involves the quantification of the uncertainty associated with each individual measurement at the elementary sampling unit (ESU) level (i.e., at Sentinel-2 spatial resolution) and incorporating these uncertainties within the upscaling process for the validation of Sentinel-3 vegetation products [10]. Whilst the methodology for upscaling in-situ reference measurements of vegetation bio-geophysical variables is well-established [4,11], until this point, the incorporation of uncertainties was not. Consequently, validation of satellite vegetation bio-geophysical products has been largely conducted through comparison with upscaled in situ reference data without explicitly accounting for the uncertainties associated with these data (e.g., [12–17]). Through incorporation of per-pixel uncertainties in the reference maps has facilitated both validation and conformity testing with respect to mission/user requirements of medium spatial resolution satellite bio-geophysical variables.

This work focuses on validation and conformity testing of two of Sentinel-3's Ocean and Land Colour Instrument (OLCI) Level 2 (L2) land products, the green instantaneous FAPAR (so-called GIFAPAR) and the CCC derived from OLCI terrestrial chlorophyll index (OTCI) with the FRM-based high-resolution reference maps generated from FRMs collected in four campaigns over agricultural (Las Tiesas—Barrax, Spain) and deciduous forest (Wytham Woods, UK) sites. Section 2 describes the FRM data collected during the campaigns, the FRM-based reference maps, the satellite products under evaluation, and the validation and conformity testing methods. Section 3 presents the results. Section 4 discusses the results, and finally, conclusions and recommendations are presented in Section 5.

2. Materials and Methods

2.1. Campaigns and Fiducial Reference Measurements

During FRM4Veg Phases 1 and 2, field campaigns were carried out in the summers of 2018 and 2021 over two study sites: Las Tiesas—Barrax (1–8 June 2018 and 19–22 July 2021) and Wytham Woods (3–12 July 2018 and 20–23 July 2021) (Figure 1). Las Tiesas–Barrax (39.0549°N, 2.1010°W) lies approximately 10 km west of Albacete, Spain and is managed by the Instituto Técnico Agronómico Provincial (ITAP). It is comprised of irrigated crops, including alfalfa, garlic, rapeseed, onion, sunflower, poppy, wheat and rainfed cereals

crops, and has been widely used for ESA Cal/Val activities. Wytham Woods (51.7734°N, 1.3384°W) is located approximately 5 km west of Oxford, UK, and is managed by the University of Oxford. It is comprised of ancient seminatural woodland (oak, ash, beech, hazel, and sycamore are the dominant species) and is one of the CEOS Working Group on Calibration and Validation (WGCV) Land Product Validation (LPV) supersites [18].
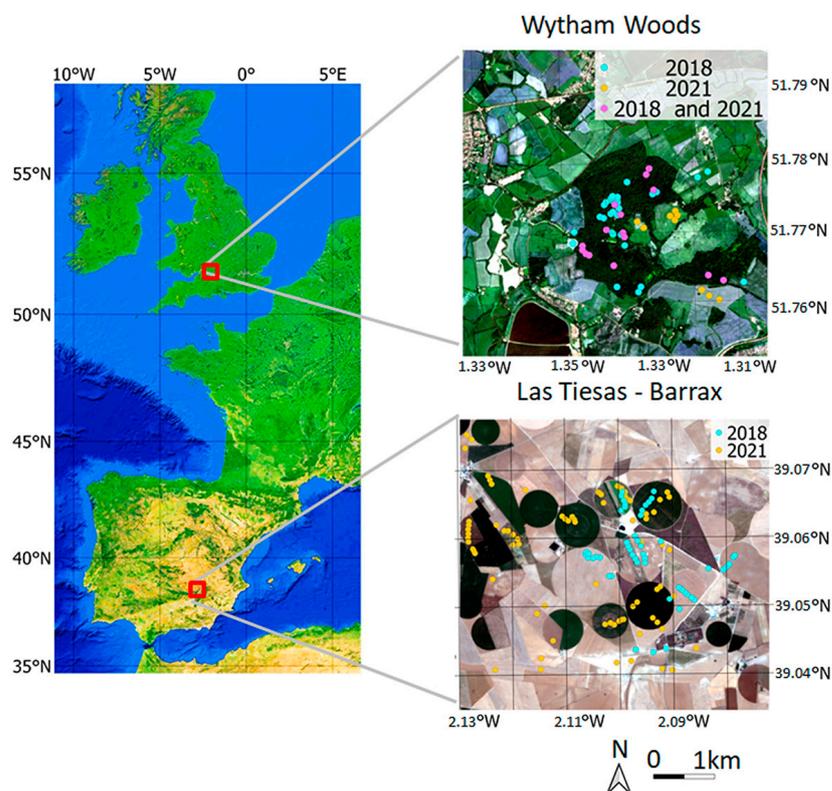

Figure 1. Location of the Las Tiesas—Barrax and Wytham Woods study sites and ESUs sampled in 2018 and 2021 campaigns. Background images for Wytham Woods and Barrax correspond to the Sentinel-2/MSI RGB colour composition in mid-July 2021.

FRMs were collected within ESUs of 20 m × 20 m containing 13 to 15 sampling locations following a regular pattern [10]. Between 48 and 79 ESUs were characterised at Las Tiesas—Barrax following stratified sampling per crop type (Figure 1 and Table 1), whereas at Wytham Woods, between 29 and 47 ESUs were characterised following a random sampling scheme (Figure 1 and Table 1). At Las Tiesas—Barrax, up to three different instruments were used to derive FAPAR and leaf area index (LAI) from measurements of gap fraction or transmittance. These included digital hemispherical photography (DHP) using either a Canon EOS 6D or 60D digital single-lens reflex camera equipped with a Sigma 8 mm F3.5 or 4.5 mm F2.8 EX DG fisheye lens, the LI-COR LAI-2200 Plant Canopy Analyser instrument [19], and the Meter Group AccuPAR LP-80 ceptometer [20]. At Wytham Woods, where the height of the woodland prevented reliable above-canopy reference readings, only DHP was used to characterise both the understory (downward-looking) and the overstory (upward-looking). DHP images were processed using CAN-EYE V6.49 [21].

Table 1. Number of ESUs sampled during each campaign.

	2018		2021	
Study Site	**FIPAR**	**CCC**	**FIPAR**	**CCC**
Las Tiesas—Barrax	52	48	79	63
Wytham Woods	47	30	29	29

It should be noted that measurements of gap fraction or transmittance strictly provide estimates of the fraction of intercepted PAR (FIPAR) rather than FAPAR. However, due to the dominant absorption of the leaves in the PAR domain, FIPAR is considered a very good approximation of the FAPAR with minor differences in most conditions [22,23]. Similarly, gap fraction measurements lead to an estimate of the Plant Area Index (PAI) rather than LAI, as there is no distinction between leaves and other elements in the canopy. PAI is very close to the LAI for crops in the early stages of maturity [22]; however, in forests, the difference can be larger due to the presence of woody material, including branches and stems, as the tree trunks are masked during the DHP processing.

Uncertainty was estimated considering several components, including instrument levelling, sampling, and image classification, as described in [10]. In addition, where reliable measurements of the same variable from more than one instrument were available (see Appendix A for an intercomparison of estimates from different instruments), the mean value was computed, and its final uncertainty was derived as the quadratic addition of (i) the uncertainty of each estimate propagated through the calculation of the mean, and (ii) the standard error of the mean (to account for the variability due to the use of different instruments).

CCC was determined as the product of LAI and leaf chlorophyll concentration (LCC), which was assessed using a Konica Minolta SPAD-502 chlorophyll meter [24,25]. Six replicate measurements were made for each sampled leaf. Relative values provided by the SPAD-502 were converted to absolute units through calibration against destructively determined LCC. At Wytham Woods, dedicated SPAD-502 calibration data were obtained, involving the collection of 60 leaves for each species [10]. At Las Tiesas—Barrax, a similar procedure was adopted using calibration data collected during a previous campaign over a similar agricultural site, in which 105 leaves were collected from a range of different crops [26]. In terms of individual in-situ LCC measurements, two sources of uncertainty were considered: those inherent to the SPAD-502 and those related to the calibration function [10]. As the mean of multiple in-situ measurements was taken to represent each ESU, the uncertainties associated with each individual observation were propagated through the calculation of the mean, whilst the standard error of the mean was calculated to reflect uncertainty due to sampling. Thus, the combined standard uncertainty in SPAD-derived LCC at the ESU level was determined by adding these two terms in quadrature [10]. Finally, the uncertainties of LCC and LAI were propagated through the calculation of the CCC. It should be noted that a reprocessing of the 2018 dataset (version 2) with the same calibration data was performed to generate a fully consistent dataset in both (2018 and 2021) campaigns.

FRMs collected at Las Tiesas—Barrax and Wytham Woods demonstrated substantial variability in FAPAR and CCC between the two sites, whilst differences between years were less pronounced (Figure 2). For FAPAR, higher and less variable values were observed at Wytham Woods, whereas at Barrax, large variability (range of variation close to 1) was observed during both years (Table 2). Whilst average CCC values were also higher at Wytham Woods than at Las Tiesas—Barrax, greater variability was observed at the former as opposed to the latter site (Figure 2 and Table 3). Regarding the uncertainties, for FAPAR, higher absolute uncertainties were observed at Las Tiesas—Barrax (mean = 0.04 to 0.10) than at Wytham Woods (mean = 0.04) across both years (Figure 2 and Table 2). This is likely a result of the increased homogeneity (and therefore reduced spatial variability) of the latter site. As expected, the same pattern was evident when the uncertainties were expressed in relative terms. It was noted that the large maximum relative uncertainty in Las Tiesas—Barrax is derived from one crop where large differences between DHP and LAI-2200 were found in 2018; the median value of 9% was representative of this site in 2018. In contrast to FAPAR, absolute CCC uncertainties were relatively consistent between the two sites and across all years (median = 0.34 g·m^{-2} to 0.40 g·m^{-2}) (Figure 2 and Table 3), except for Las Tiesas—Barrax in 2021 (median = 0.15 g·m^{-2}). However, due to the larger CCC values

experienced at Wytham Woods, relative CCC uncertainties were smaller (median = 21% to 22%) than at Las Tiesas—Barrax (median = 29% to 25%) (Figure 2 and Table 3).
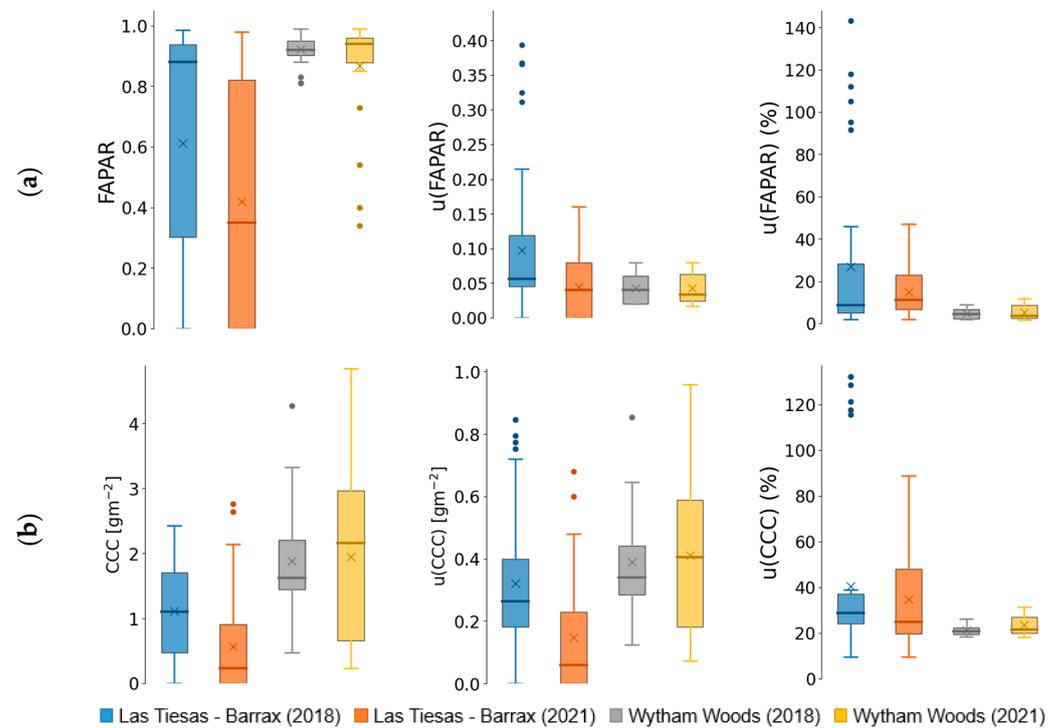

Figure 2. Box plots of fiducial reference values and their absolute and relative uncertainties (at the k = 2 coverage factor) for the 2018 and 2021 campaigns at Las Tiesas—Barrax agricultural site and Wytham Woods deciduous forest site for (**a**) FAPAR and (**b**) CCC. These values correspond to version 2 for the 2018 data with consistent LAI processing and chlorophyll calibration coefficients with the 2021 campaign.

Table 2. Summary statistics for fiducial reference FAPAR values and their associated absolute and relative uncertainties (at the k = 2 coverage factor, which indicates 95.4% confidence) from the 2018 and 2021 field campaigns at Las Tiesas—Barrax and Wytham Woods.

	FAPAR (Dimensionless)				U(FAPAR) (Dimensionless)			
	Barrax 2018	**Barrax 2021**	**Wytham 2018**	**Wytham 2021**	**Barrax 2018**	**Barrax 2021**	**Wytham 2018**	**Wytham 2021**
Minimum	0.00	0.00	0.81	0.34	<0.01 (2.0%)	<0.01 (2.0%)	0.02 (2.0%)	0.02 (1.7%)
Maximum	0.99	0.98	0.99	0.99	0.39 (143.0%)	0.16 (47.1%)	0.08 (9.1%)	0.08 (11.8%)
Mean	0.61	0.42	0.92	0.87	0.10 (27.0%)	0.04 (14.8%)	0.04 (4.7%)	0.04 (5.4%)
Median	0.88	0.35	0.92	0.94	0.06 (8.8%)	0.04 (11.1%)	0.04 (4.4%)	0.03 (3.5%)
STD	0.36	0.38	0.04	0.18	0.10 (35.3%)	0.04 (11.8%)	0.02 (2.2%)	0.02 (3.4%)

Table 3. Summary statistics for fiducial reference CCC values and their associated absolute and relative uncertainties (at the k = 2 coverage factor) from the 2018 and 2021 field campaigns at Las Tiesas—Barrax and Wytham Woods.

	CCC (g·m^{-2})				U(CCC) (g·m^{-2})			
	Barrax 2018	**Barrax 2021**	**Wytham 2018**	**Wytham 2021**	**Barrax 2018**	**Barrax 2021**	**Wytham 2018**	**Wytham 2021**
Minimum	0.00	0.00	0.47	0.23	0.00 (9.5%)	0.00 (9.7%)	0.12 (18.3%)	0.07 (18.2%)
Maximum	2.43	2.76	4.27	4.84	0.85 (132.2%)	0.68 (88.9%)	0.85 (26.3%)	0.96 (31.5%)
Mean	1.11	0.56	1.88	1.94	0.32 (40.6%)	0.15 (34.7%)	0.39 (21.3%)	0.41 (23.6%)
Median	1.10	0.23	1.62	2.16	0.26 (28.9%)	0.06 (24.8%)	0.34 (20.8%)	0.40 (21.5%)
STD	0.78	0.75	0.84	1.35	0.23 (35.1%)	0.18 (22.0%)	0.15 (2.1%)	0.26 (4.4%)

2.2. FRM-Based Sentinel-2 Reference Maps

FRMs collected in the 2018 and 2021 campaigns were upscaled using Sentinel-2 Multi-spectral Instrument (MSI) imagery, acquired within one week of the in situ data collection, to generate FRM-based high-spatial resolution reference maps for validation and conformity testing. The upscaling approach incorporates the estimation of the uncertainties in the FRM-based reference maps as described in [10]. First, the Sentinel-2 Radiometric Uncertainty Tool (RUT) [27,28] was adopted to estimate per-pixel uncertainties associated with the L1C top-of-atmosphere reflectance values. Orthogonal distance regression (ODR) was then used to derive the transfer function for upscaling, accounting for uncertainties in both satellite and in-situ reference data. Transfer functions were derived between FRMs and two vegetation indices: the normalised difference vegetation index (NDVI) for FAPAR and the Sentinel-2 terrestrial chlorophyll index (S2TCI) for CCC [10]. Finally, a categorical quality flag layer was produced to identify areas in which the transfer function was acting as an extrapolator (and, therefore, might provide less reliable outputs) [29]. The comparison of upscaled values with the FRM data shows relative RMSD of between 6% and 28% for FAPAR and between 43% and 72% for CCC, with systematic differences for some crops (see Appendix B). The higher discrepancies for CCC are expected due to the larger uncertainties in the CCC measurements (as these incorporate the uncertainties in both the LAI and LCC measurements).

The FRM-based high-resolution reference maps for FAPAR (Figure 3) and CCC (Figure 4) over the study sites allow the easy identification of crop patterns at Las Tiesas—Barrax and cultivated and forest areas at Wytham Woods. Las Tiesas—Barrax demonstrates a mix of large areas with very low values (bare soil or fallow fields) and irrigated crops with dense to very dense vegetation. On the other hand, at Wytham Woods, the forest area is located at the centre of the image, and it is surrounded by crops, grassland and some water bodies. For comparative purposes, the propagated uncertainty at a coverage factor k = 2 (i.e., 95.4% confidence) and the relative uncertainty of reference maps over the ESUs are shown for FAPAR (Table 4) and CCC (Table 5). Median uncertainties over the ESUs range between 0.02 and 0.03 for FAPAR and between 0.18 g·m^{-2} and 0.57 g·m^{-2} for CCC. Median relative uncertainties range between 2.6% and 6.4% for FAPAR and between 24% to 43% for CCC. The uncertainties associated with the FAPAR reference maps are relatively low (typically lower than the FRM data) mainly because the linear relationship shows very low uncertainty, as does the TOA NDVI used for upscaling. However, for CCC, reference map uncertainties are larger than the uncertainties of FRM data.
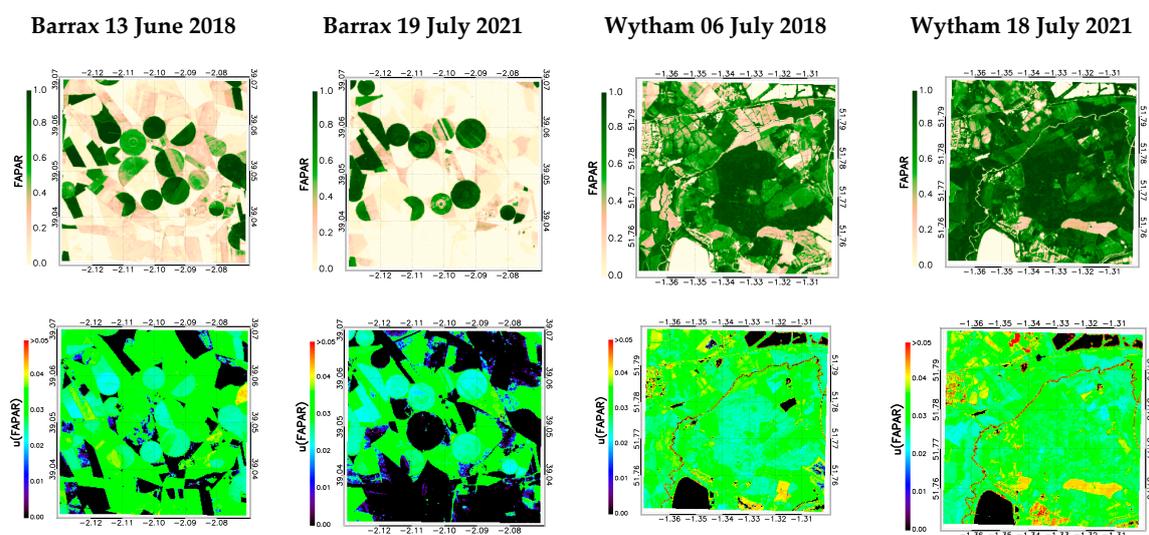

Figure 3. FAPAR FRM-based reference maps (**top**) and uncertainties at the k = 2 coverage factor (**bottom**) over Las Tiesas—Barrax agricultural and Wytham Woods deciduous forest sites (5 km × 5 km). Imagery Sentinel-2A/MSI.

Barrax 13 June 2018   **Barrax 19 July 2021**   **Wytham 06 July 2018**   **Wytham 18 July 2021**
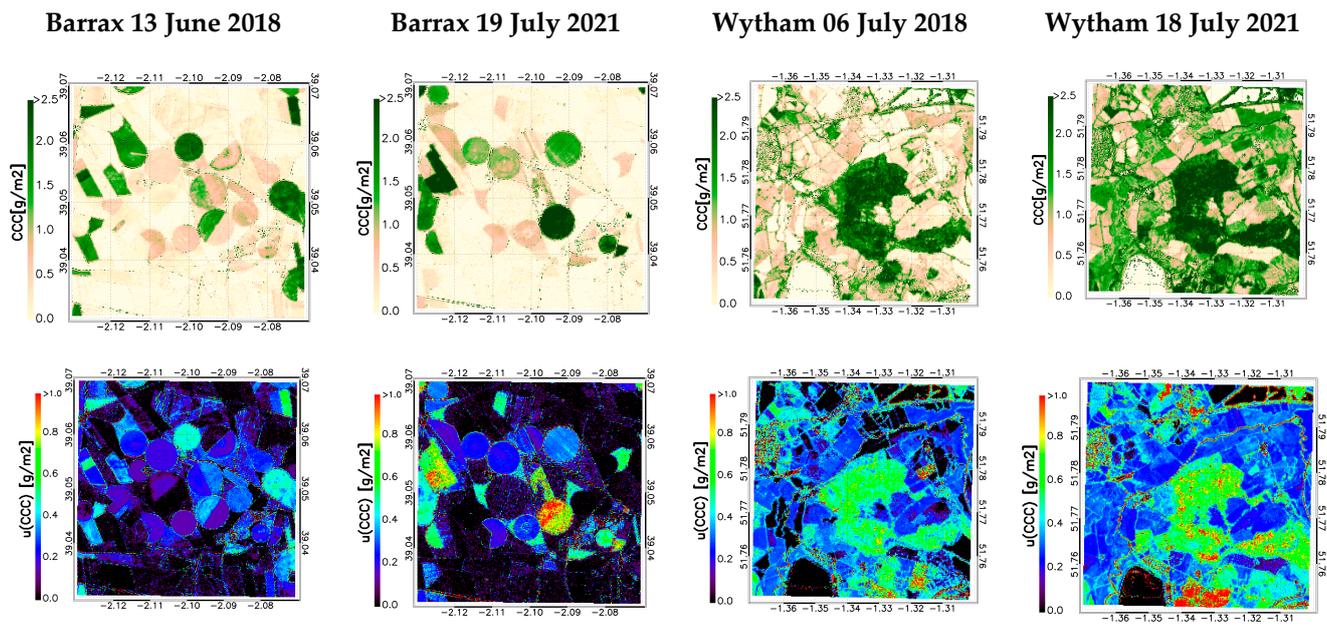

Figure 4. CCC FRM-based reference maps (**top**) and uncertainties at the k = 2 coverage factor (**bottom**) over Las Tiesas—Barrax agricultural and Wytham Woods deciduous forest sites (5 km × 5 km). Imagery Sentinel-2A/MSI.

Table 4. Summary statistics for FAPAR FRM-based reference maps and their associated absolute and relative uncertainties (at the k = 2 coverage factor) over ESU locations from the 2018 and 2021 field campaigns at Las Tiesas—Barrax and Wytham Woods. Maximum uncertainties are restricted to 50%.

	FAPAR (Dimensionless)				U(FAPAR) (Dimensionless)			
	Barrax 2018	**Barrax 2021**	**Wytham 2018**	**Wytham 2021**	**Barrax 2018**	**Barrax 2021**	**Wytham 2018**	**Wytham 2021**
Minimum	0.00	0.00	0.00	0.20	0.00 (2.5%)	0.00 (2.0%)	0.00 (2.3%)	0.02 (2.3%)
Maximum	0.98	1.00	0.98	1.00	0.03 (50.0%)	0.04 (50.0%)	0.04 (50.0%)	0.04 (21.0%)
Mean	0.53	0.43	0.85	0.83	0.02 (12.9%)	0.02 (13.7%)	0.02 (4.3%)	0.03 (5.1%)
Median	0.55	0.33	0.95	0.94	0.03 (5.1%)	0.02 (6.4%)	0.02 (2.6%)	0.03 (3.0%)
STD	0.36	0.38	0.28	0.25	0.01 (17.7%)	0.01 (16.4%)	0.01 (8.0%)	0.01 (5.2%)

Table 5. Summary statistics for CCC FRM-based reference maps and their associated absolute and relative uncertainties (at the k = 2 coverage factor) over ESU locations from the 2018 and 2021 field campaigns at Las Tiesas—Barrax and Wytham Woods. Maximum relative uncertainties are restricted to 50%.

	CCC (g·m^{-2})				U(CCC) (g·m^{-2})			
	Barrax 2018	**Barrax 2021**	**Wytham 2018**	**Wytham 2021**	**Barrax 2018**	**Barrax 2021**	**Wytham 2018**	**Wytham 2021**
Minimum	0.00	0.00	0.00	0.10	0.00 (17.3%)	0.00 (16.8%)	0.00 (22.0%)	0.05 (19.2%)
Maximum	2.32	3.36	3.01	3.50	0.52 (50.0%)	0.99 (50.0%)	0.78 (50.0%)	0.96 (50.0%)
Mean	0.83	0.73	2.06	1.84	0.22 (34.7%)	0.23 (38.1%)	0.52 (26.5%)	0.47 (30.4%)
Median	0.75	0.37	2.31	2.20	0.22 (34.1%)	0.18 (42.7%)	0.56 (24.0%)	0.57 (26.0%)
STD	0.78	0.92	0.72	1.09	0.18 (13.0%)	0.27 (12.6%)	0.16 (7.3%)	0.27 (10.3%)

2.3. Sentinel-3 OLCI Bio-Geophysical Products

OLCI instruments are currently operational aboard two Copernicus Sentinel-3 (A and B) satellites, orbiting the Earth on sun-synchronous polar orbits with a mean altitude of 815 km and a local equatorial crossing time of 10:00 am. The spectral range of the OLCI instrument is 400–1040 nm, divided into 21 spectral bands [30]. Two different Sentinel-3 OLCI L2 land products are considered: (i) the green instantaneous FAPAR (GIFAPAR) (Section 2.3.1) and (ii) the OLCI terrestrial chlorophyll index (OTCI) (Section 2.3.2), a surrogate of CCC. The GIFAPAR and OTCI products are provided at the native Sentinel-3 OLCI resolution (300 m, i.e., full resolution) and at degraded spatial resolution (1 km, i.e., reduced resolution).

2.3.1. GIFAPAR

The GIFAPAR (so-called OLCI Global Vegetation Index—OGVI) product is designed to provide continuity to the Medium Resolution Imaging Spectrometer (MERIS) Global Vegetation Index (MGVI). GIFAPAR exploits the fact that live green vegetation strongly absorbs solar radiation in the red region of the electromagnetic spectrum and strongly scatters it in the near-infrared region. The product is designed to maximise sensitivity to instantaneous green FAPAR whilst minimising sensitivity to perturbing factors such as atmospheric contamination and the soil background. The underlying algorithm, developed by the Joint Research Centre (JRC), consists of two main steps [31]. In the first, 'rectified' reflectance values are computed from OLCI bands 17 (865 nm) and 10 (681.25 nm). The rectification procedure uses information from OLCI band 3 (442.5 nm) to suppress atmospheric effects, whilst directional normalisation is carried out using the parametric Rahman-Pinty-Verstraete (RPV) model [32]. In the second step, the 'rectified' reflectance values are used to derive FAPAR following an optimisation procedure. Both steps are achieved with ratios of polynomials, making use of sensor-specific coefficients (see details at [33]). The GIFAPAR is provided with per-pixel uncertainties. Two main terms are considered for the uncertainty: the propagation error and the optimisation error [33]. Note that L1 uncertainty is not implemented in the OLCI processing chain yet, hence the current uncertainty budget should correspond to the optimisation error. Figure 5 shows the Sentinel-3B GIFAPAR values and its uncertainty for Las Tiesas—Barrax agricultural and Wytham Woods sites over the study area of 5 km × 5 km for the 2018 and 2021 campaigns.
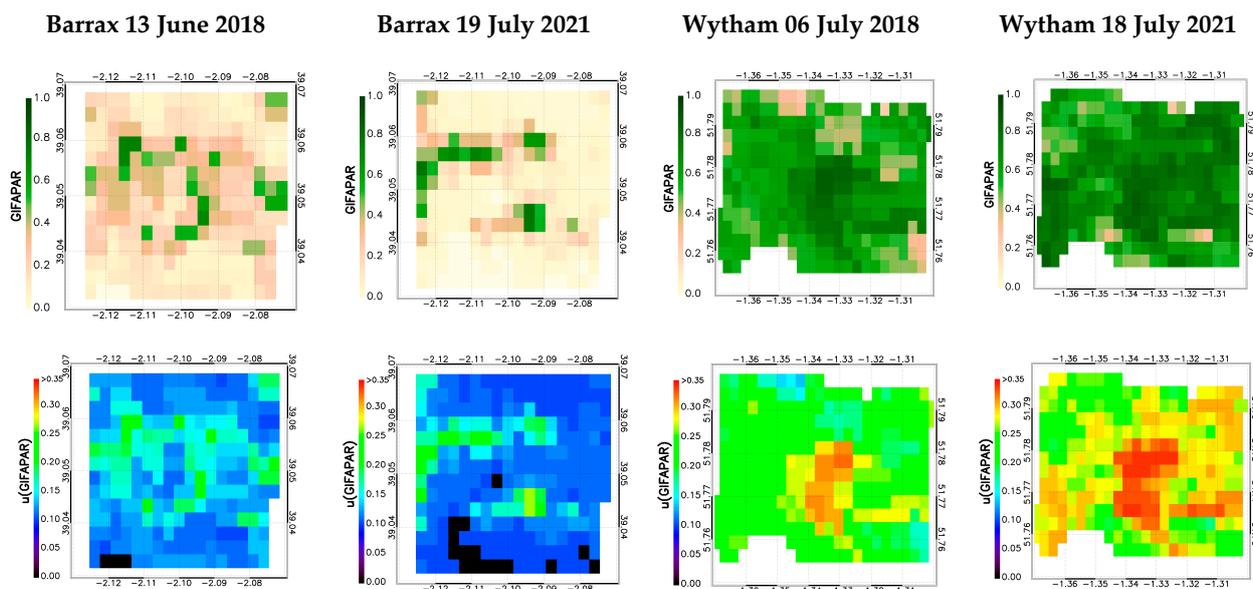

Figure 5. Sentinel-3B GIFAPAR values (**top**) and uncertainties at the k = 2 coverage factor (**bottom**) over Las Tiesas—Barrax and Wytham Woods sites for 12 June 2018 and 6 July 2021. The images cover an extension of 5 km × 5 km. GIFAPAR pixels with no data are displayed in white.

2.3.2. OTCI—CCC

The OTCI is a unique chlorophyll index for OLCI data designed to provide continuity to the MERIS Terrestrial Chlorophyll Index (MTCI). The interaction of incoming radiation with a vegetated surface results in a distinctive reflectance spectrum. As the key photosynthetic pigment in plants, chlorophyll absorbs much of the incoming radiation in the visible region of the electromagnetic spectrum, leading to low reflectance. In the near-infrared, optical properties are mostly controlled by leaf structure, and reflectance in this region of the electromagnetic spectrum is high due to internal scattering within the leaf. The boundary between strong absorption due to the presence of chlorophyll and strong reflectance due to leaf structure is known as the red edge, and its position (i.e., the location of the maximum rate of change) is strongly related to CCC [34]. As CCC increases, the red edge moves towards longer wavelengths.

Taking advantage of the MERIS red-edge bands, the MTCI was designed to provide a computationally efficient surrogate of CCC that remains sensitive to high CCC values [35]. Based on the MTCI, the OTCI is calculated from equivalent OLCI bands in and around the red edge as

$$\text{OTCI} = \frac{R_{b12} - R_{b11}}{R_{b11} - R_{b10}}, \tag{1}$$

where R_{b12}, R_{b11}, and R_{b10} are reflectance values in the OLCI bands centred at 753.75 nm, 708.75 nm, and 681.25 nm, respectively, after correction for gaseous absorption and Rayleigh scattering [36]. As for OGVI, the OTCI algorithm can provide per-pixel uncertainties, which are derived by propagating uncertainties in the input quantities through its calculation. At the time of writing this manuscript, however, L1 uncertainties are yet to be implemented in the OLCI processing chain and therefore, it is not possible to estimate uncertainty for L2 OTCI products. This is expected to be available in a future reprocessing of the product.

Sentinel-3 CCC maps were derived by calibrating the OTCI product with CCC FRM-based reference maps according to a linear function, using ODR to account for uncertainties. The FRM-based Sentinel-2 reference maps were aggregated to OLCI's native spatial resolution using its effective point spread function (PSF) as described in Section 2.5. Due to the differences introduced by vegetation type, the calibration of OTCI was achieved per site using the CCC reference maps from both campaigns. The slope (α) and intercept (β) values and their uncertainties provided by the ODR regression method are shown in Table 6. Finally, the uncertainties of the slope and intercept are propagated through the calibration function to obtain the uncertainty of the CCC as follows:

$$\text{OTCI} = \alpha\,\text{CCC} + \beta \tag{2}$$

$$\text{CCC} = \frac{\text{OTCI} - \beta}{\alpha} \tag{3}$$

$$u(\text{CCC}) = \sqrt{\left(\frac{\text{OTCI} - \beta}{\alpha^2}\right)^2 u^2(\alpha) + \left(\frac{1}{\alpha}\right)^2 u^2(\beta)} \tag{4}$$

The resulting CCC maps and their uncertainties are displayed in Figure 6 for Sentinel-3B acquisitions.
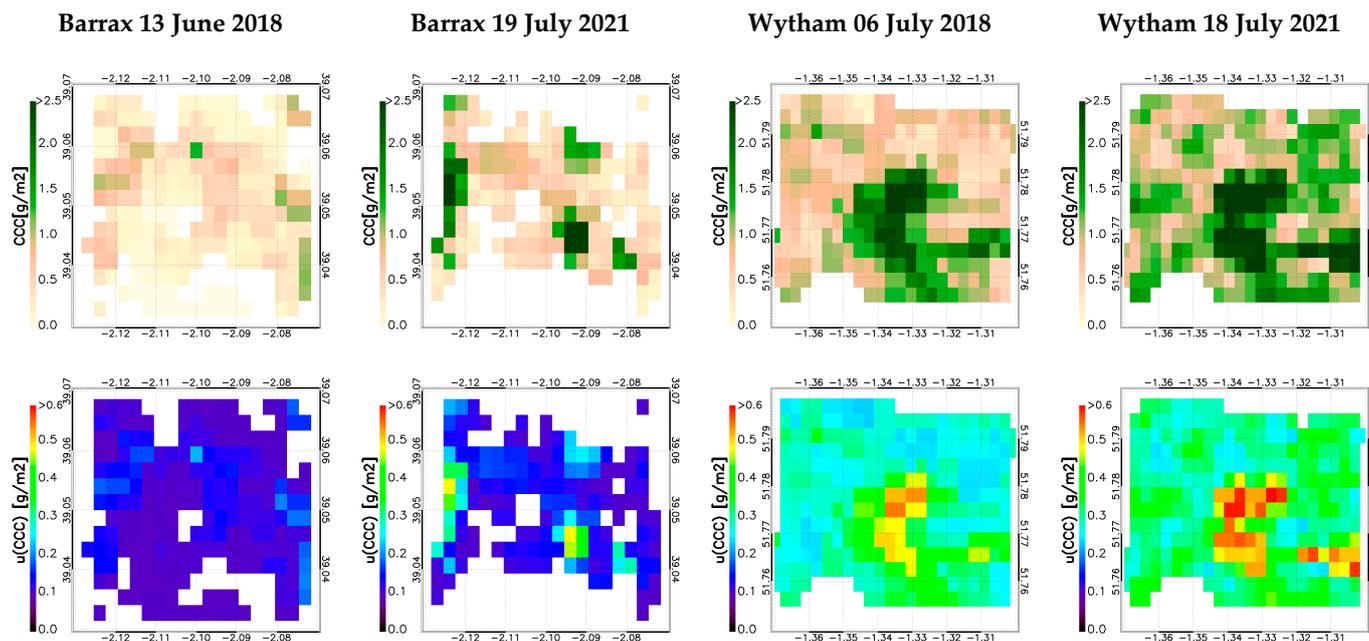
Figure 6. Sentinel-3B CCC values (**top**) and uncertainties at the k = 2 coverage factor (**bottom**) over Las Tiesas-Barrax and Wytham Woods sites derived from Sentinel-3B OTCI. OTCI/CCC pixels with no data, mostly related to soil and no vegetation, are displayed in white.

Table 6. Sentinel-3B CCC calibration coefficients derived from Sentinel-3B OTCI and FRM-based reference maps using ODR.

	α	β
Las Tiesas—Barrax	1.70 ± 0.13	1.23 ± 0.08
Wytham Woods	0.87 ± 0.08	1.48 ± 0.10

2.4. Validation and Conformity Testing

Validation is the process of independently assessing and evaluating the quality of the data products from the system outputs [3]. In the satellite-based land product context, validation refers to the assessment and quantification of the accuracy and uncertainties of the product with respect to reference datasets. The accuracy, precision, and uncertainty of the Sentinel-3 OLCI bio-geophysical products under study are evaluated by several metrics. The accuracy, which represents the systematic errors, is often computed as the statistical mean bias (B) or the median deviation (MD). Precision, which represents the dispersion of the retrievals around their expected value, is often computed using standard deviation (STD) or the median absolute deviation (MAD). Uncertainty, a nonnegative parameter associated with the result of a measurement that characterises the dispersion of the quantity values being attributed to a measurand [37], is often characterised using the root mean square deviation (RMSD). In addition to these metrics, the Pearson correlation coefficient and the ODR slope and intercept line are included as indicative of the correlation between both datasets and the bias, respectively. It should be noted that for the evaluation of OTCI-based CCC products, a leave-one-out cross-validation (denoted by "cv") method was used.

Conformity testing is the process that determines if the estimated quantities are within the range of tolerable values or not [6]. In this work, Sentinel-3 OLCI bio-geophysical products are evaluated with respect to Sentinel-3's mission requirements [38]. In particular, the goal (<5%) and threshold (<10%) requirements on accuracy are considered for both GIFAPAR and CCC at full resolution, even though, strictly speaking, the threshold requirements are defined at 1 km spatial resolution. It should be noted that in the case of chlorophyll products, mission requirements indicate that OTCI from Sentinel-3 should be

within 5% of OTCI measured on the ground (not CCC). However, as OTCI is used as a surrogate measure of CCC (which is a key bio-geophysical variable), the mission requirements for OTCI are being tested as if they were applicable for CCC (as for FAPAR or LAI). This should be clarified in future mission requirements for Sentinel-3 Next Generation.

Traditionally, uncertainties in satellite and reference data were assumed negligible in conformity testing (i.e., it was assumed that all data points within the tolerance interval defined by the requirements conform, and all data points outside this tolerance interval do not conform). This decision rule is known as simple acceptance. However, when satellite and reference data uncertainties are well characterised, conformity can be asserted if a data point and its uncertainty are fully contained within the tolerance interval (in order to reduce the risk of accepting a non-conforming entity). In this case, the decision rule is called guarded acceptance, as the probability of false acceptance or false rejection is reduced [39].

Thus, given a candidate satellite product, $(Q_i \pm u(Q_i))$, and a best estimate or reference, $(R_i \pm u(R_i))$, the apparent error (ε_i) and its uncertainty $u(\varepsilon_i)$ can be estimated as follows [6]:

$$\varepsilon_i = Q_i - R_i, \tag{5}$$

$$u(\varepsilon_i) = \sqrt{u(Q_i)^2 + u(R_i)^2}, \tag{6}$$

The distribution of the uncertainty is assumed to be Gaussian, and the coverage factor (k) is typically set to 2 to obtain an expanded uncertainty with a confidence interval of 95.4%. In this study, $k = 2$ is used. Δ represents the maximum permissible error, given by the Sentinel-3 mission requirements, during the conformity test and each pixel i can be classified into four categories (Figure 7):

- Conclusively conforming (guarded acceptance): If the apparent error absolute value and its expanded uncertainty are lower or equal to the maximum permissible error:

$$|\varepsilon_i \pm ku(\varepsilon_i)| \leq \Delta \tag{7}$$

- Conclusively non-conforming (guarded rejection): If the apparent error absolute value and its expanded uncertainty are greater than the maximum permissible error:

$$|\varepsilon_i| > \Delta \ \& \ |\varepsilon_i \pm ku(\varepsilon_i)| > \Delta \tag{8}$$

- Inconclusively conforming: If the apparent error absolute value is lower or equal to the maximum permissible error, but the expanded uncertainty is greater than the maximum permissible error:

$$|\varepsilon_i| \leq \Delta \ \& \ (|\varepsilon_i + ku(\varepsilon_i)| \ or \ |\varepsilon_i - ku(\varepsilon_i)|) > \Delta \tag{9}$$

- Inconclusively non-conforming: If the apparent error absolute value is greater than the maximum permissible error, but the expanded uncertainty is lower or equal to the maximum permissible error:

$$|\varepsilon_i| > \Delta \ \& \ |\varepsilon_i \pm ku(\varepsilon_i)| < \Delta \tag{10}$$
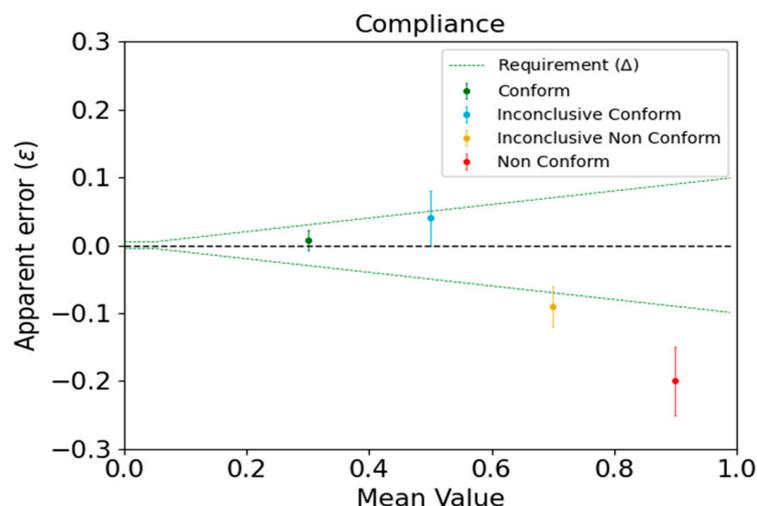
Figure 7. Illustration of conformity testing pixel classification possibilities, where the green dashed line represents the mission requirement or maximum permissible error (Δ).

2.5. Aggregation of FRM-Based Reference Maps to OLCI's Native Resolution

Finally, to be able to compare the Sentinel-3 L2 products with the FRM-based Sentinel-2 reference maps, the reference maps at 20 m spatial resolution must be aggregated to OLCI's native spatial resolution (i.e., 300 m). In order to partly account for the PSF of the OLCI sensor and the adjacency effects, an iterative data-driven method was used. Weighted averages of high spatial resolution pixels were computed by the convolution of a two-dimensional Gaussian function [40]. The weights represented the apparent PSF, considering that each hectometric pixel is composed of a limited number of decametric pixels. The method accounts for several factors that introduce differences in the comparison of satellite products (including the sensor's PSF, viewing geometry and geolocation uncertainty, as well as the effects of reprojection and atmospheric scattering) [41]. To characterise OLCI's apparent PSF, different combinations of the full-width (extension of the pixel size given by Xmax and Ymax) and the full-width at half-maximum (FWHMx and FWHMy) of the Gaussian function in both x and y directions, are iteratively tested as in [42], considering a maximum full-width in both directions of 900 m (i.e., 3 OLCI full resolution pixels). Finally, the Gaussian function, which maximises the correlation coefficient between the aggregated reference maps and Sentinel-3 products, is chosen. Two Gaussian functions were finally selected, one per site under study (Table 7). Uncertainties of each observation in the reference maps were propagated through the calculation of the mean using the same PSF functions, whilst the standard error of the mean was calculated to account for the uncertainty due to the spatial heterogeneity. The standard uncertainty of the reference maps aggregated to 300 m was finally computed by adding these two terms in quadrature.

Table 7. Optimal apparent PSF parameters used to aggregate FRM-based high spatial reference maps (20 m) to Sentinel-3 OLCI's native spatial resolution (300 m) per site and variable. X_{max} (respectively Y_{max}) represents the full width of the PSF in the east-west direction (respectively north–south). $FWHM_x$ (respectively $FWHM_y$) represents the full-width at half-maximum in the east–west direction (respectively north–south).

	X_{max} (m)	Y_{max} (m)	$FWHM_x$ (m)	$FWHM_y$ (m)
Barrax	900	450	540	450
Wytham	900	750	720	450

3. Results

Both Sentinel-3A and -3B products were evaluated against FRM-based reference maps over the Las Tiesas—Barrax agricultural and Wytham Woods deciduous forests sites. For the sake of brevity, only the validation and conformity testing results for Sentinel-3B are presented here, as those obtained from Sentinel-3A products are very similar (see Appendix C).

3.1. Agricultural Site
3.1.1. GIFAPAR

Validation of GIFAPAR over Las Tiesas—Barrax (Figure 8) demonstrates a good correlation of 0.91 with an overall RMSD of 0.11 (Table 8). GIFAPAR products tend to provide systematically negative bias (-0.06) with a slope of the linear fit of 0.69. Similar scattering is observed for both campaigns (2018 and 2021). Conformity testing (at coverage factor $k = 2$) reveals large uncertainties in the apparent error (Figure 8), with most cases classed as inconclusively non-conforming (73.7% and 70.9% for goal and threshold requirements, respectively) and with no cases conclusively conforming with the Sentinel-3 mission requirements (Table 8). However, conclusively, non-conforming pixels represent between 15% and 17% of the total number of cases, depending on the requirement.
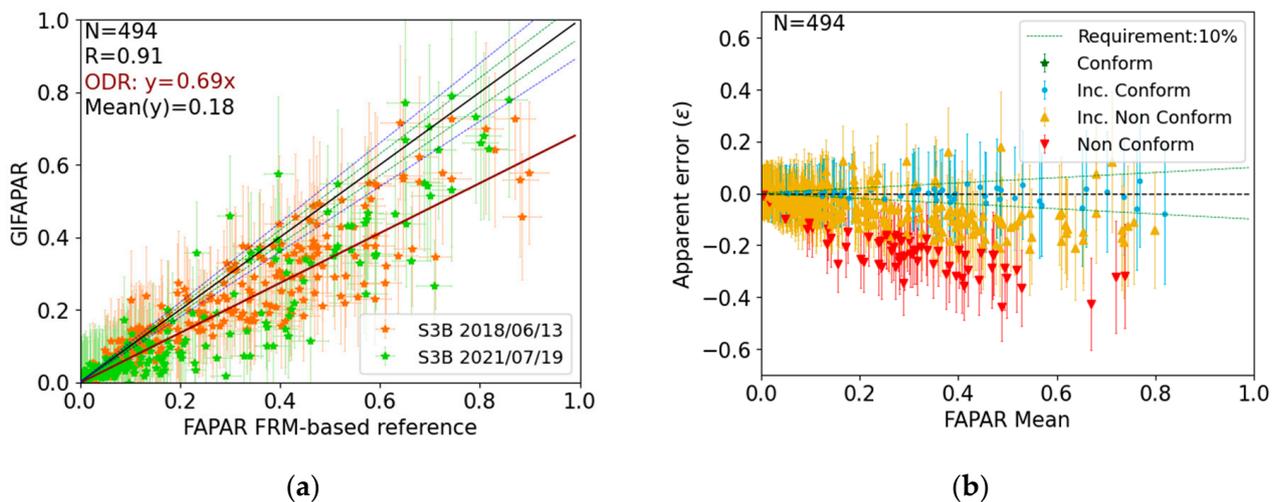

(**a**)   (**b**)

Figure 8. (**a**) Scatterplot between Sentinel-3B GIFAPAR and FRM-based reference maps over Las Tiesas—Barrax. Vertical and horizontal bars display expanded uncertainties at coverage factor $k = 2$. The dashed green and blue lines display the 5% and 10% requirement, the brown line displays the ODR fit. (**b**) Conformity testing (at $k = 2$) results regarding the Sentinel-3 mission requirements on accuracy. The dashed green line displays the 10% threshold requirement.

Table 8. Summary of validation metrics (relative values between brackets) and conformity testing according to the Sentinel-3 mission requirements on accuracy for Sentinel-3B GIFAPAR over Barrax at coverage factor $k = 2$.

Validation Metric		Requirement on Accuracy	Compliance (%)	
N	494		Conclusively conforming	0.0
R	0.91		Inconclusively conforming	8.9
ODR	Y = 0.69x	Goal (5%)	Inconclusively non-conforming	73.7
B	-0.06 (-28.7%)		Conclusively non-conforming	17.4
MD	-0.03 (-13.3%)		Conclusively conforming	0.0
STD	0.09 (44.8%)		Inconclusively conforming	14.6
MAD	0.04 (17.9%)	Threshold (10%)	Inconclusively non-conforming	70.9
RMSD	0.11 (53.2%)		Conclusively non-conforming	14.6

3.1.2. CCC

Validation results of the Sentinel-3 OTCI-based CCC products over Las Tiesas—Barrax demonstrates a good correlation (0.82) (Figure 9), with an $RMSD_{cv}$ of 0.29 g·m^{-2} and no mean bias, as expected for empirically calibrated relationships (Table 9). However, the bias seems to be slightly positive for the 2021 campaign and negative for the 2018 campaign. The slope of the ODR fit is 0.79, which indicates an overall negative bias in agreement with the median deviation (MD = −0.04). Conformity testing (Figure 9 and Table 9) shows that between 45% and 51% of pixels are conclusively non-conforming, depending on the requirement, and the rest of the cases are inconclusive. In the case of inconclusive cases, most of them are inconclusively non-conforming (around 45% of cases), and only between 6% and 10% are inconclusively conforming. This is a clear indication of the very strict requirements.
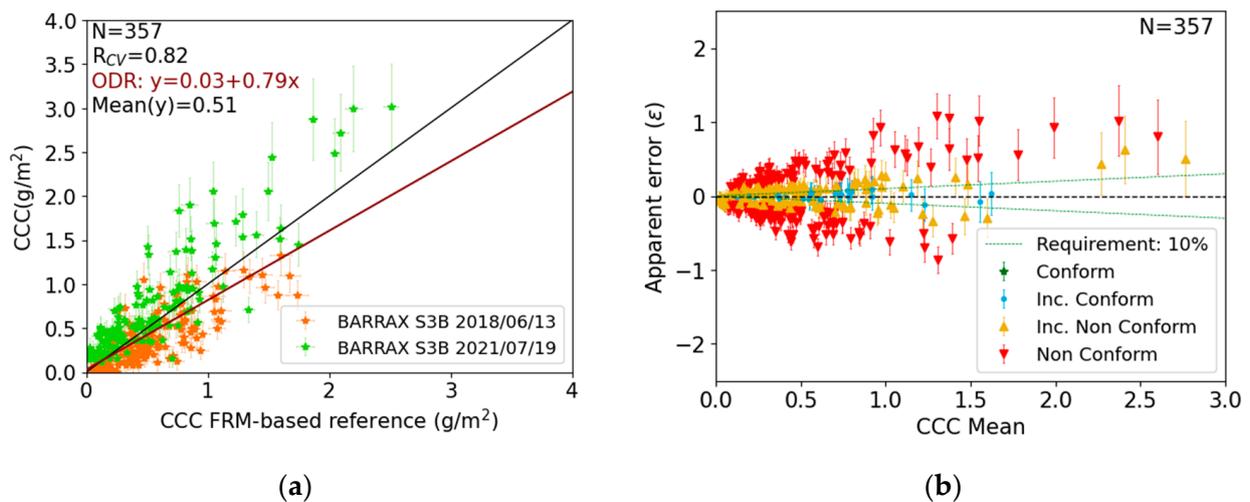

(**a**)   (**b**)

Figure 9. (**a**) Scatterplot between Sentinel-3B OTCI-based CCC and FRM-based reference maps over Las Tiesas—Barrax. Vertical and horizontal bars display expanded uncertainties at coverage factor k = 2. The dashed green and blue lines display the 5% and 10% requirement, the brown line displays the ODR fit. (**b**) Conformity testing (at k = 2) results regarding the Sentinel-3 mission requirements on accuracy. The dashed green line displays the 10% threshold requirement.

Table 9. Summary of validation metrics (cv stands for cross-validation) and conformity testing according to the Sentinel-3 mission requirements on accuracy for Sentinel-3B OTCI-based CCC over Barrax at coverage factor k = 2.

Validation Metric		Requirement on Accuracy	Compliance (%)	
N	357		Conclusively conforming	0.0
R_{cv}	0.82	Goal (5%)	Inconclusively conforming	5.6
ODR	Y = 0.03 + 0.79x		Inconclusively non-conforming	43.7
B_{cv}	0.00 (0.7%)		Conclusively non-conforming	50.7
MD_{cv}	−0.04 (−7.1%)		Conclusively conforming	0.0
STD_{cv}	0.29 (56.3%)	Threshold (10%)	Inconclusively conforming	10.1
MAD_{cv}	0.15 (28.8%)		Inconclusively non-conforming	44.5
$RMSD_{cv}$	0.29 (56.3%)		Conclusively non-conforming	45.4

3.2. Deciduous Forest Site

3.2.1. GIFAPAR

Validation results of Sentinel-3B GIFAPAR over Wytham Woods (Figure 10 and Table 10) demonstrate a correlation of 0.85, RMSD of 0.1 and mean negative bias (and MD) of -0.06 (approximately 9% in relative terms). Similar scatterplots are observed for the two campaigns with systematic deviations from the 1:1 line for the highest values, which corresponds to the wooded areas. Conformity testing reveals very large uncertainties (at k = 2) in the apparent error, mostly coming from the large uncertainties from the satellite product (Figure 10). Consequently, almost all cases (around 99%) are inconclusive, with none of the samples conclusively conforming to the mission requirements. For the inconclusive samples, around half of the samples are inconclusively conforming and the other half are inconclusively non-conforming with respect to the 10% threshold requirement.
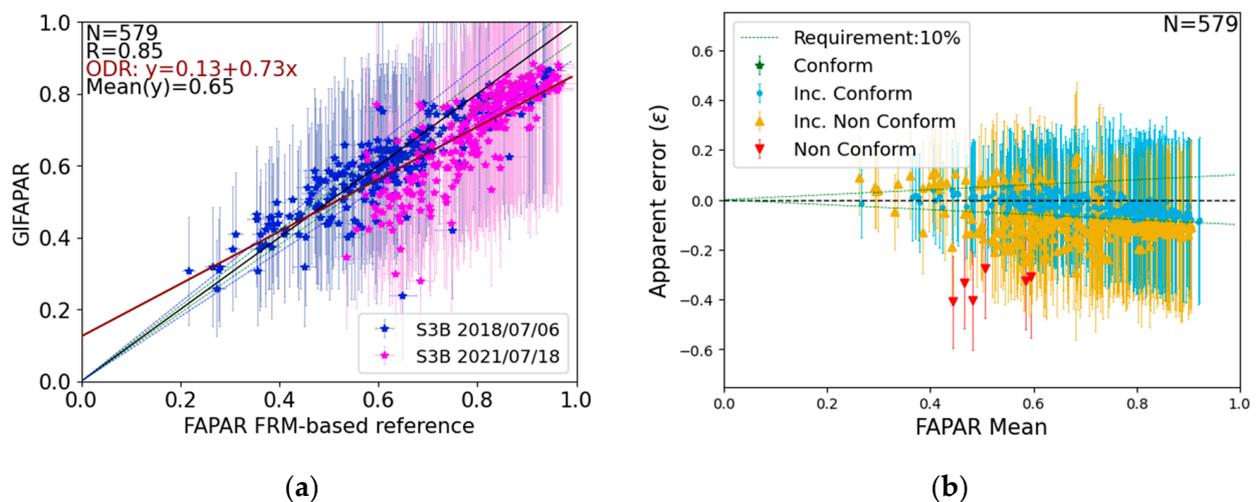
| (**a**) | (**b**) |

Figure 10. (**a**) Scatterplot between Sentinel-3B GIFAPAR and FRM-based reference maps over Wytham Woods. Vertical and horizontal bars display expanded uncertainties at coverage factor k = 2. The dashed green and blue lines display the 5% and 10% requirement, the brown line displays the ODR fit. (**b**) Conformity testing (at k = 2) results regarding the Sentinel-3 mission requirements on accuracy. The dashed green line displays the 10% threshold requirement.

Table 10. Summary of validation metrics and conformity testing according to the Sentinel-3 mission requirements on accuracy for Sentinel-3B GIFAPAR over Wytham Woods at coverage factor k = 2.

Validation Metric		Requirement on Accuracy	Compliance (%)	
N	579		Conclusively conforming	0.0
R	0.85	Goal (5%)	Inconclusively conforming	24.0
ODR	Y = 0.13 + 0.73x		Inconclusively non-conforming	74.8
B	-0.06 (-8.7%)		Conclusively non-conforming	1.2
MD	-0.06 (-9.0%)		Conclusively conforming	0.0
STD	0.08 (11.6%)	Threshold (10%)	Inconclusively conforming	48.4
MAD	0.07 (10.1%)		Inconclusively non-conforming	50.6
RMSD	0.10 (14.5%)		Conclusively non-conforming	1.0

3.2.2. CCC

The validation of OTCI-based CCC products over Wytham Woods (Figure 11) demonstrates a high correlation of 0.88 and RMSD of 0.28 g·m^{-2}. As observed for Las Tiesas—Barrax, almost no mean bias is found, but MD is also close to zero, and the slope of the linear fit is close to 0.9 (Table 11). The conformity testing shows again that most cases are inconclusive, with inconclusively non-conforming cases accounting for 69.7% and 57.4%,

considering goal and threshold uncertainty requirements of 5% and 10%, respectively. Conclusively, non-conforming pixels represent between 10% and 15% of the total, depending on the requirement.
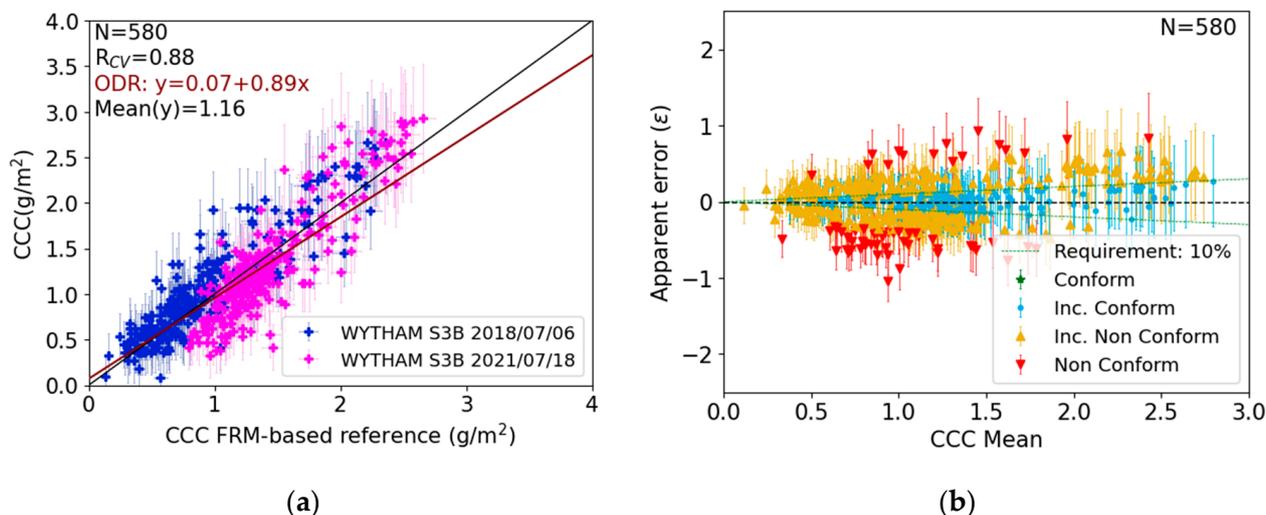

(**a**) (**b**)

Figure 11. (**a**) Scatterplot between Sentinel-3B OTCI-based CCC and FRM-based reference maps over Wytham Woods. Vertical and horizontal bars display expanded uncertainties at coverage factor k = 2. The dashed green and blue lines display the 5% and 10% requirement, the brown line displays the ODR fit. (**b**) Conformity testing (at k = 2) results regarding the Sentinel-3 mission requirements on accuracy. The dashed green line displays the 10% threshold requirement.

Table 11. Summary of validation metrics (cv stands for cross-validation) and conformity testing according to the Sentinel-3 mission requirements on accuracy for Sentinel-3B OTCI-based CCC over Wytham Woods at coverage factor k = 2.

Validation Metric		Requirement on Accuracy	Compliance (%)	
N	580		Conclusively conforming	0.0
R_{cv}	0.88		Inconclusively conforming	15.3
ODR	Y = 0.07 + 0.89x	Goal (5%)	Inconclusively non-conforming	69.7
B_{cv}	<0.01 (<0.1%)		Conclusively non-conforming	15.0
MD_{cv}	0.01 (1.2%)		Conclusively conforming	0.0
STD_{cv}	0.28 (24.3%)		Inconclusively conforming	31.9
MAD_{cv}	0.17 (14.7%)	Threshold (10%)	Inconclusively non-conforming	57.4
$RMSD_{cv}$	0.28 (24.3%)		Conclusively non-conforming	10.7

3.3. Overall Results

3.3.1. GIFAPAR

Overall validation results of Sentinel-3B GIFAPAR with all FRM-based reference maps demonstrate a remarkably high correlation of 0.96, even though some scatter is observed mainly for the more heterogeneous Las Tiesas—Barrax site (Figure 12). The GIFAPAR product demonstrates an overall RMSD of 0.1 (23%) and accuracy (bias) of −0.06 (−13%) (Table 12). The systematic negative bias is also observed in the linear fit with a slope of 0.84. Very similar results were obtained from Sentinel-3A observations (Appendix C). The overall conformity testing shows inconclusive results in more than 90% of cases (Table 12). Considering the 10% threshold level, up to 32% of the samples are inconclusively conforming, but only 17% of the samples are inconclusive conforming in the case of the 5% goal requirement. None of the samples conclusively conform to the Sentinel-3 mission requirements on accuracy.
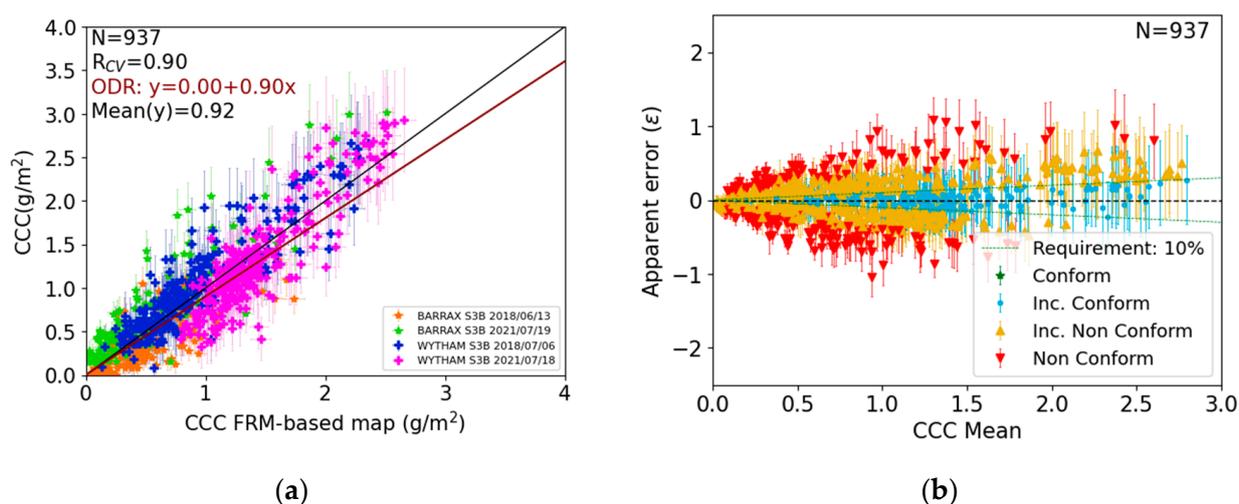
(**a**)

(**b**)

Figure 12. (**a**) Scatterplot between Sentinel-3B GIFAPAR and FRM-based reference maps for Las Tiesas-Barrax (crosses) and Wytham Woods (stars) sites. Vertical and horizontal bars display expanded uncertainties at coverage factor k = 2. The dashed green and blue lines display the 5% and 10% requirement, the brown line displays the ODR fit. (**b**) Conformity testing (at k = 2) results regarding the Sentinel-3 Mission Requirements on accuracy. The dashed green line displays the 10% threshold requirement.

Table 12. Summary of validation metrics and conformity testing according to the ESA Sentinel-3 Mission requirements on accuracy for Sentinel-3B GIFAPAR at coverage factor k = 2.

Validation Metric		Requirement on Accuracy	Compliance (%)	
N	1073		Conclusively conforming	0.0
R	0.96		Inconclusively conforming	17.1
ODR	Y = 0.84x	Goal (5%)	Inconclusively non-conforming	74.3
B	−0.06 (−12.8%)		Conclusively non-conforming	8.7
MD	−0.05 (−10.3%)		Conclusively conforming	0.0
STD	0.09 (18.5%)		Inconclusively conforming	32.8
MAD	0.06 (12.6%)	Threshold (10%)	Inconclusively non-conforming	59.9
RMSD	0.10 (22.5%)		Conclusively non-conforming	7.3

3.3.2. CCC

The overall validation of Sentinel-3 OTCI-based CCC products with reference maps for both sites also demonstrates a high correlation of 0.9 (as for GIFAPAR). The RMSD is 0.28 g·m^{-2}, and there is almost no bias (mean bias and MD close to zero). The linear fit shows a slope of 0.9, which reveals a slight tendency to underestimate the ground reference data, even though the OTCI-based CCC displays the opposite trend for high values (>2 g·m^{-2}) (Figure 13). The conformity testing (Table 13) shows that most of the cases are inconclusive (>70%). As observed for GIFAPAR, none of the samples conclusively conform to the Sentinel-3 mission requirements, and conclusively, non-conforming samples represent between 24% and 29% of the total, depending on the requirement.

(**a**)

(**b**)

Figure 13. (**a**) Scatterplot between Sentinel-3B OTCI-based CCC and FRM-based reference maps for Las Tiesas—Barrax (crosses) and Wytham Woods (stars) sites. Vertical and horizontal bars display expanded uncertainties at coverage factor k = 2. The black line corresponds to the 1:1 and the brown line displays the ODR fit. (**b**) Conformity testing (at **k** = 2) results regarding the Sentinel-3 mission requirements on accuracy. The dashed green line displays the 10% threshold requirement.

Table 13. Summary of validation metrics and conformity testing according to the Sentinel-3 mission requirements on accuracy for Sentinel-3B OTCI-based CCC at coverage factor k = 2.

	Validation Metric	Requirement on Accuracy	Compliance (%)	
N	937		Conclusively conforming	0.0
R	0.90	Goal (5%)	Inconclusively conforming	11.6
ODR	Y = 0.90x		Inconclusively non-conforming	59.8
B	<0.01 (0.2%)		Conclusively non-conforming	28.6
MD	−0.01 (−0.6%)		Conclusively conforming	0.0
STD	0.28 (31.0%)	Threshold (10%)	Inconclusively conforming	23.6
MAD	0.16 (17.5%)		Inconclusively non-conforming	52.5
RMSD	0.28 (31.0%)		Conclusively non-conforming	23.9

4. Discussion

4.1. Performance of the Products

The GIFAPAR products derived either from Sentinel-3A or -3B show a good overall performance compared with the FRM-based reference maps, with a high correlation (>0.9) and an RMSD of 0.1 (0.11) for Sentinel-3A (-3B). However, there is a systematic underestimation of the reference values (median deviation of −0.05, slope of the linear fit of 0.84), which is more evident for high FAPAR values. These results are in agreement with the evaluation of the Sentinel-3 GIFAPAR using Copernicus Ground-Based Observations for Validation (GBOV) upscaled FIPAR reference data, among others [43]. Part of this underestimation is explained by the differences in the FAPAR definition between satellite estimates and in-situ values. GIFAPAR is defined as green instantaneous FAPAR, whereas our FRMs, derived from DHP, LAI-2200 PCA or ceptometers, are defined as instantaneous FIPAR ("green" only in case of DHP downward-looking images, i.e., over crops). It is well-known that FIPAR is a good proxy of FAPAR [22,23]; however, it may overestimate it. The difference between FIPAR and FAPAR depends on illumination, soil background and the amount of chlorophyll in the leaves. Wojnowski et al. [44] reported low differences (about 6–9%) at high chlorophyll levels for all background and illumination conditions considered for individual trees. In comparison, FIPAR can be up to 20–25% higher than FAPAR for leaves with low chlorophyll content [44]. Similarly, the differences between FIPAR and FAPAR

should be higher in forests due to the impact of the woody material in the ground measurements. It can be observed in Wytham Woods that the systematic differences between our FRM-based references and the GIFAPAR are larger for the highest values corresponding to the wooded areas. The differences between the total absorbed value and that of the foliage can be simulated by the use of three-dimensional radiative transfer (3D-RT) models in order to correct the bias due to the presence of woody material [43,45], but this requires additional effort to collect spectral and structural measurements to parameterise the 3D-RT model. Recent work has also demonstrated the potential of near-infrared DHP for assessing woody material [46], and the use of this technique would allow the PAR intercepted by woody material to be subtracted from the total FIPAR to derive foliage FIPAR. Conformity testing against Sentinel-3 mission uncertainty requirements provides mostly inconclusive results, with around half of the cases inconclusively non-conforming and the other half inconclusively conforming regarding the threshold level, with not a single case conclusively conforming with mission requirements. These results are partly due to the large uncertainties provided with the GIFAPAR product when compared to the strict mission requirements, particularly for very low values. As such, the product uncertainty requirements and attainable reference data uncertainty are discussed hereafter.

There was a strong correlation between CCC derived from OTCI and the FRM-based reference maps for the four dedicated campaigns. Sentinel-3A CCC has a slightly lower performance in terms of RMSD than Sentinel-3B, largely due to the systematic differences of CCC in Sentinel-3A at the Wytham Woods site (see Appendix C). The reason for this is still under investigation. It is worth noting that the ground measurements of CCC have a much larger inherent uncertainty associated with them, in some cases more than 50% of the measured values. This is because CCC is a product of LAI and LCC, and uncertainty from both of these measurements propagates through to the final uncertainty of CCC, thus making the overall uncertainty larger (details are provided in [23]). This large ground data uncertainty impacts the upscaling function and the corresponding Sentinel-2-derived FRM map. For conformity testing, the uncertainty requirements for OTCI (and FAPAR) are interpreted as the same for CCC, and, therefore, it is tested against 5% (goal) and 10% (threshold). No Sentinel-3A or -3B pixels conclusively met those requirements, with most of them falling into the inconclusively non-conforming category.

4.2. Mission Requirements and Attainable Reference Data Uncertainty

Uncertainty requirements are associated with the majority of bio-geophysical products, in the form of mission requirements [38], as well as user or community requirements, such as those specified by the Global Climate Observing System (GCOS) and Sentinels for Science (SEN4SCI) programmes [15,47]. For FAPAR and CCC (OTCI), current requirements range from 5% to 20% relative uncertainty and should be expressed with an absolute uncertainty requirement (as in GCOS) for very small values. If compliance with these requirements is to be reliably assessed, the reference data used for conformity testing must have an equal (or ideally lower) uncertainty to these requirements [6].

Our results indicate that the expanded uncertainties (at 95.4% confidence) associated with FRM could exceed product uncertainty requirements, with median relative expanded uncertainties of between 4% and 11% for FAPAR and 21% to 29% for CCC (see Section 2.1). These results reflect similar claims made in previous studies for bio-geophysical variables such as LAI [13,15,48,49]. It is worth noting that these ESU level uncertainties are further increased by upscaling (due to the addition of radiometric uncertainty associated with the high spatial resolution imagery and the uncertainty associated with the transfer function used in upscaling itself), with median relative uncertainties between 3% and 6% for FAPAR and 24% to 43% for CCC (see Section 2.2). In the case of FAPAR, similar uncertainties compared to the in situ data are obtained because of the low radiometric uncertainties of the TOA NDVI (<1%) used as input to the transfer function for upscaling. However, the large uncertainties associated with the CCC high spatial resolution reference maps lead to a situation in which compliance cannot be conclusively confirmed or denied. Even if

the random uncertainties are significantly reduced during the aggregation to hectometric resolution, the systematic uncertainties remain. Further, additional sources of uncertainties should be considered in the high spatial resolution reference maps, such as those introduced by the upscaling approach (e.g., regressions with vegetation indices versus calibrated RT models [50]) or by the sampling of the site [51]. Moreover, uncertainties related to the validation approach, including those introduced by geolocation errors and the mismatch between satellite pixels and the reference maps, can be larger than requirements over heterogenous landscapes [51].

This is even more problematic, considering that the uncertainty associated with satellite products can also exceed the mission requirements. For GIFAPAR, the expanded uncertainties over densely vegetated targets are larger than 30%, which explains by itself that conformity testing against 5–10% requirements provides inconclusive results. The uncertainties of the GIFAPAR product need to be further evaluated [43]. On the other hand, OTCI uncertainties were not yet disseminated at the time of this research, and the results presented here correspond only to the uncertainties in the CCC estimation.

5. Conclusions

In this work, FRM data from four campaigns over two vegetated sites (Las Tiesas—Barrax and Wytham Woods), coupled with an end-to-end uncertainty estimation procedure, have been utilised to validate two Sentinel-3 L2 bio-geophysical products: GIFAPAR and OTCI-based CCC. For the first time, it is performed conformity testing to evaluate if these products meet Sentinel-3 mission requirements (i.e., 5% goal, and 10% threshold). In the absence of any specific requirements for a CCC product, it is assumed that the requirements for OTCI are similar to those for a CCC product. In general, both GIFAPAR and CCC (derived from OTCI) were strongly related to upscaled ground measurements, with little variation between Sentinel-3A and -3B products. GIFAPAR shows correlations >0.95, RMSD ~ 0.1 and a slight negative bias (~-0.06) for both sites. This bias could be partly explained by the differences in the FAPAR definitions between satellite estimates and FRMs references. For the OTCI-based CCC, leave-one-out cross-validation demonstrated correlations >0.8 and RMSDcv ~0.28 g·m^{-2}. However, despite de encouraging validation results, none of the products conclusively met the mission requirements on accuracy set by ESA, with most cases providing inconclusive results (typically in more than 90% of cases for GIFAPAR and more than 75% of cases for CCC). Considering the complexity of the ground measurements, heterogeneity at the moderate resolution pixel scale, and challenges with the upscaling, the existing mission requirements are strict and would be difficult to confirm with the two-stage validation approach. Moreover, the uncertainties attached to the satellite product can be larger than the requirements.

Therefore, as a next step in EO-based vegetation product validation and conformity testing, it is recommended: (i) reviewing the current mission requirements and setting more realistic requirements at least at the threshold level using both absolute (for very low values) and relative terms, (ii) setting procedures to undertake conformity testing at the decametric and the hectometric scales by directly comparing with spatially representative FRM to avoid the two-stage validation approach uncertainties, and (iii) using innovative ground measurement techniques such as terrestrial laser scanning, which avoids dependency on illumination conditions, subjective classification and levelling to a large extent, and explore the potential of UAV-mounted hyperspectral instrument to reduce reference measurement uncertainty. Phase 3 of FRM4Veg will allow these latter two points to be explored.

Author Contributions: Conceptualization, F.C., L.A.B., J.D., N.O. and V.B.; methodology, F.C., E.M.-S., L.A.B., J.S.-Z. and J.D.; software, E.M.-S. and L.A.B.; investigation, F.C., E.M.-S., L.A.B., J.S.-Z. and J.D.; data curation, J.S.-Z., E.M.-S., L.A.B., H.M., O.W. and R.M.; writing—original draft preparation, F.C., E.M-S. and J.S.-Z.; writing—review and editing, F.C., E.M.-S., L.A.B., J.S.-Z., J.D., N.O., H.M. and R.M.; project administration, F.C., J.D., L.A.B., N.O. and V.B.; funding acquisition, V.B., F.C., J.D., L.A.B. and N.O. All authors have read and agreed to the published version of the manuscript.

Appendix A. Intercomparison of FAPAR and LAI Retrieved from LAI 2200 PCA, AccuPAR and DHP

During the Las Tiesas—Barrax campaign in 2021, FAPAR and LAI (for CCC retrievals) were estimated using DHP, LAI-2200 PCA and AccuPAR LP-80 instruments. The average value of the quality-controlled data was used for the upscaling. Figure A1 shows the scatterplots for FAPAR retrievals, and Figure A2 shows the scatterplots for LAI retrievals between the three instruments.
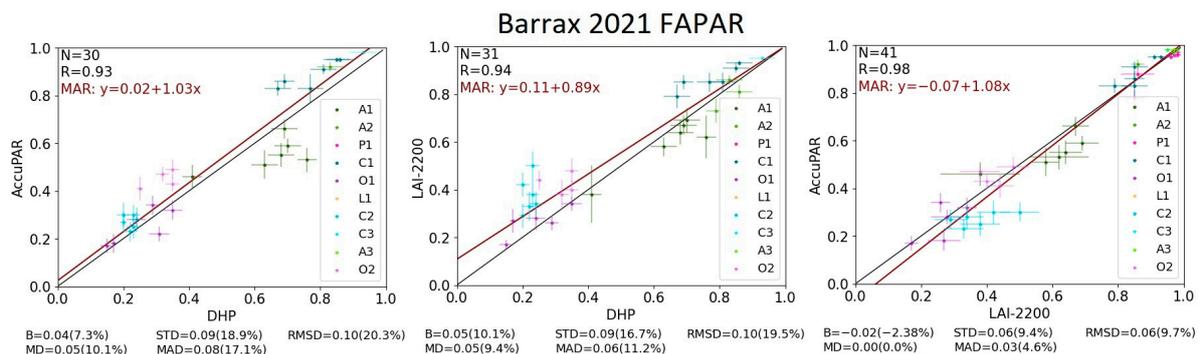

Figure A1. Scatterplots of FAPAR retrievals and uncertainties between different instruments: AccuPAR and DHP (**left**), LAI-2200 and DHP (**middle**), AccuPAR and LAI-2200 (**right**). The black line displays the 1:1 relationship, the brown line displays the MAR fit. In the legend, "A" stands for Alfalfa, "P" for Pepper, "C" for Corn, "O" for Onion, and "L" for Lettuce. Numbers refer to different fields.
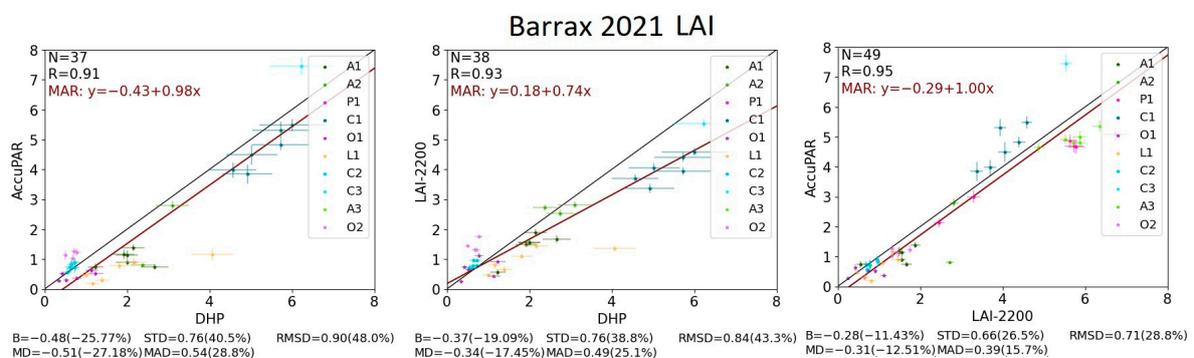

Figure A2. Scatterplots of LAI measurements and uncertainties between different instruments: AccuPAR and DHP (**left**), LAI-2200 and DHP (**middle**), AccuPAR and LAI-2200 (**right**). The black line displays the 1:1 relationship, the brown line displays the MAR fit. In the legend, "A" stands for Alfalfa, "P" for Pepper, "C" for Corn, "O" for Onion, and "L" for Lettuce. Numbers refer to different fields.

Appendix B. Performance of the FRM-Based Upscaled Reference Maps with In-Situ FRM

The FRM-based high spatial resolution upscaled values are compared against the in-situ FRM, and validation metrics are computed for the four campaigns: two over Las Tiesas—Barrax (Figure A3) and two over Wytham Woods (Figure A4).
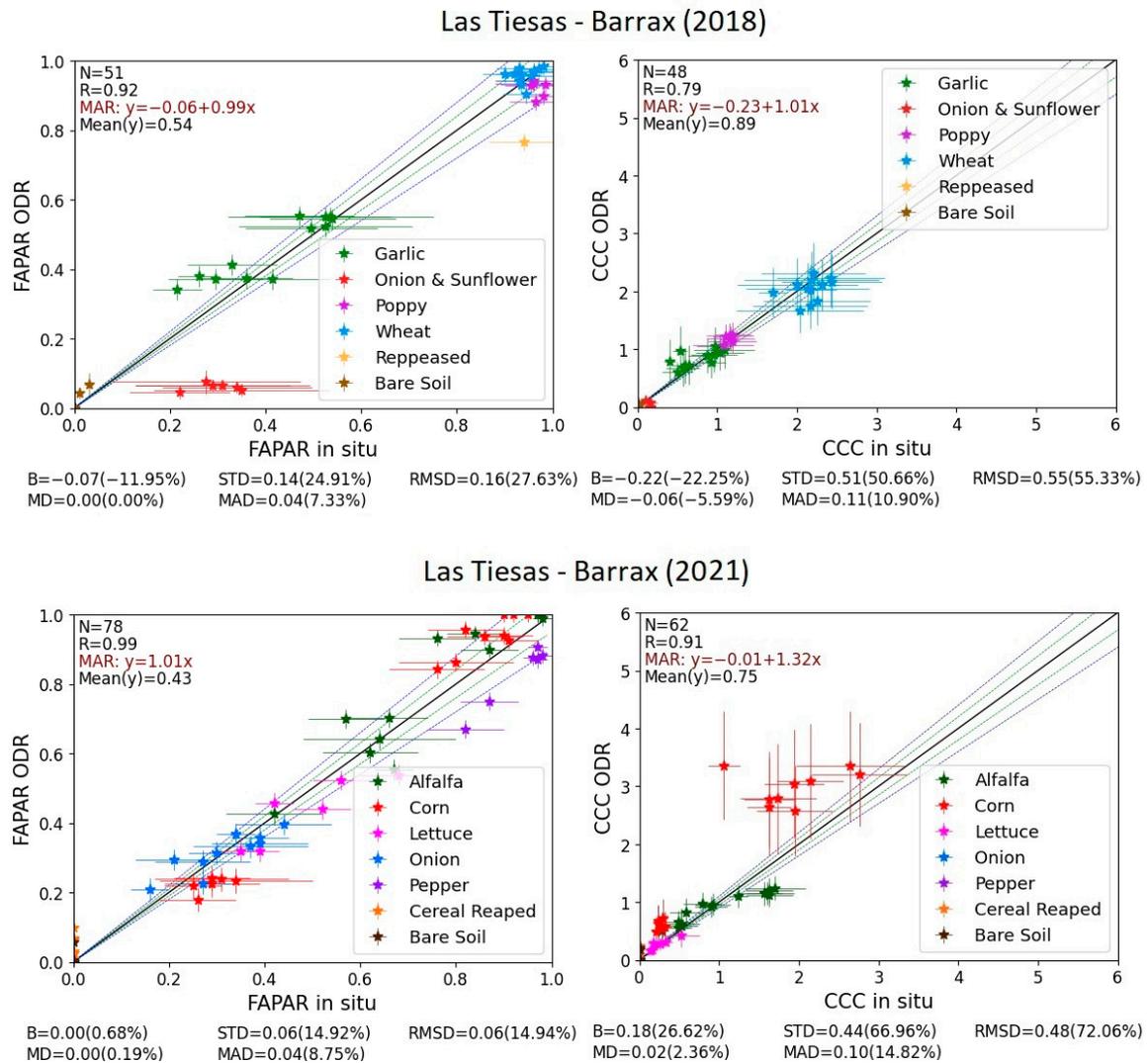

Figure A3. Comparison between high spatial resolution reference maps and in-situ FRM of FAPAR and CCC ($g \cdot m^{-2}$) from the 2018 (**top**) and 2021 (**bottom**) campaigns at Las Tiesas—Barrax. Error bars correspond to the expanded uncertainties at coverage factor k = 2 (95.4% confidence). The dashed green and blue lines display the 5% and 10% requirement, the black line displays the 1:1 relationship.
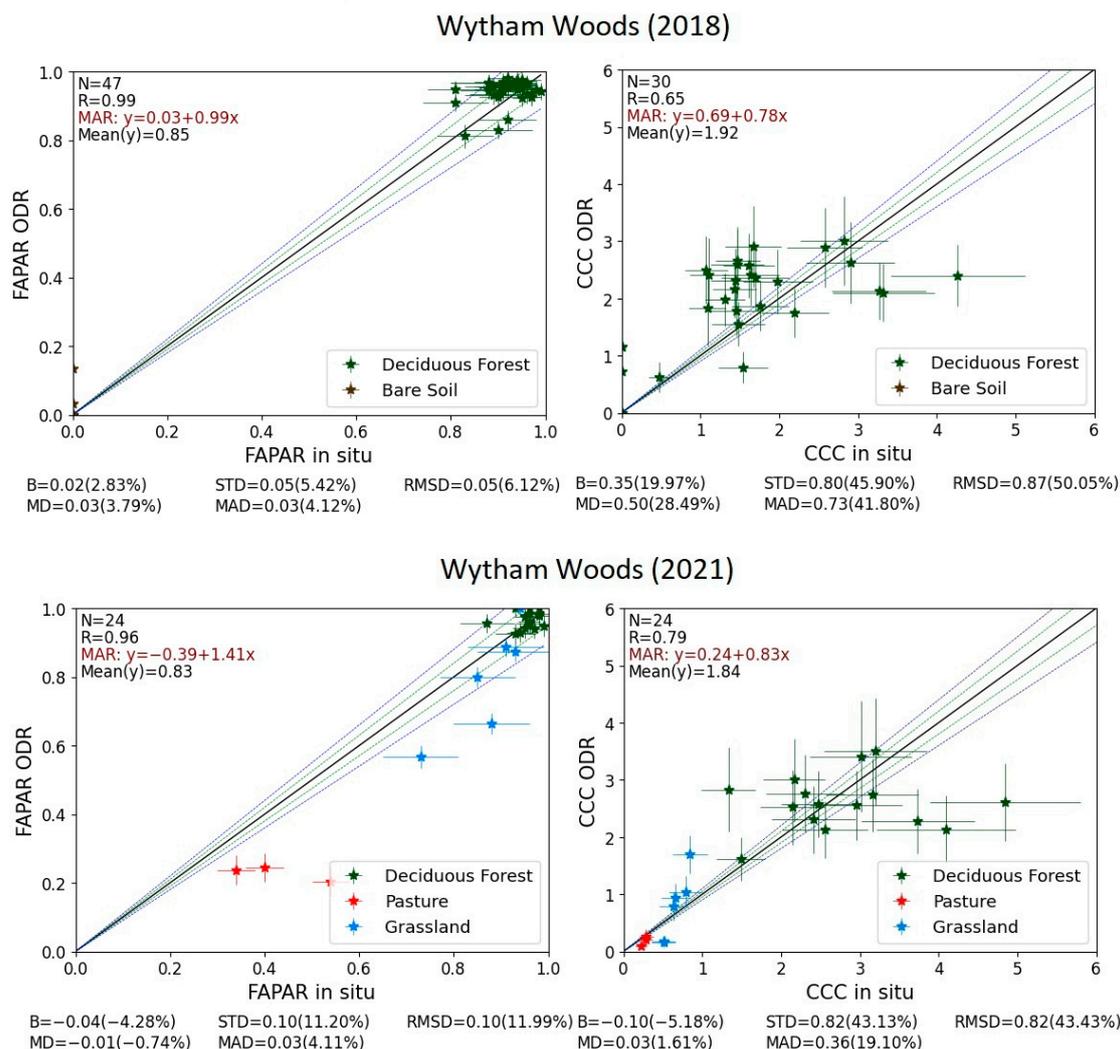
Figure A4. Comparison between high spatial resolution reference maps and in-situ FRM of FAPAR and CCC (g·m^{-2}) from the 2018 (**top**) and 2021 (**bottom**) campaigns at Wytham Woods. Error bars correspond to the expanded uncertainties at coverage factor k = 2 (95.4% confidence). The dashed green and blue lines display the 5% and 10% requirement, the black line displays the 1:1 relationship.

Appendix C. Overall Validation and Conformity Testing Results for Sentinel-3A GIFAPAR and OTCI-Based CCC

This appendix shows the overall validation and conformity testing results for the Sentinel-3A products. The same procedure as for the Sentinel-3B products was followed but using the calibration coefficients of Table A1.

Table A1. Sentinel-3A CCC calibration coefficients derived from Sentinel-3B OTCI and FRM-based reference maps using ODR.

	α	β
Las Tiesas—Barrax	1.66 ± 0.14	1.25 ± 0.09
Wytham Woods	0.66 ± 0.08	1.61 ± 0.10

(**a**)   (**b**)
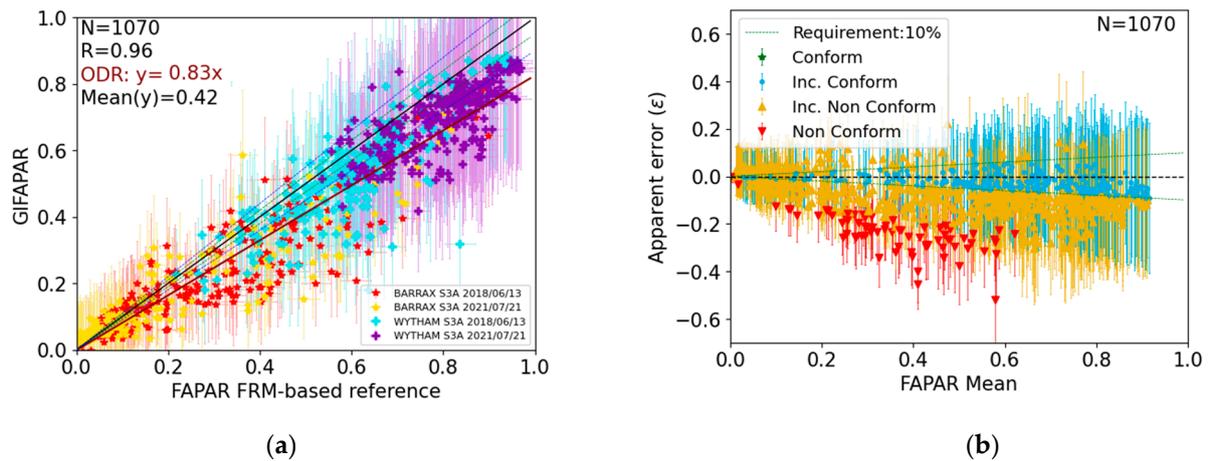
Figure A5. (**a**) Scatterplot between Sentinel-3A GIFAPAR and FRM-based reference maps for Las Tiesas—Barrax (crosses) and Wytham Woods (stars) sites. Vertical and horizontal bars display expanded uncertainties at coverage factor k = 2. The brown line displays the ORD fit. (**b**) Conformity testing (at k = 2) results regarding the Sentinel-3 mission requirements on accuracy. The dashed green line displays the 10% threshold requirement.
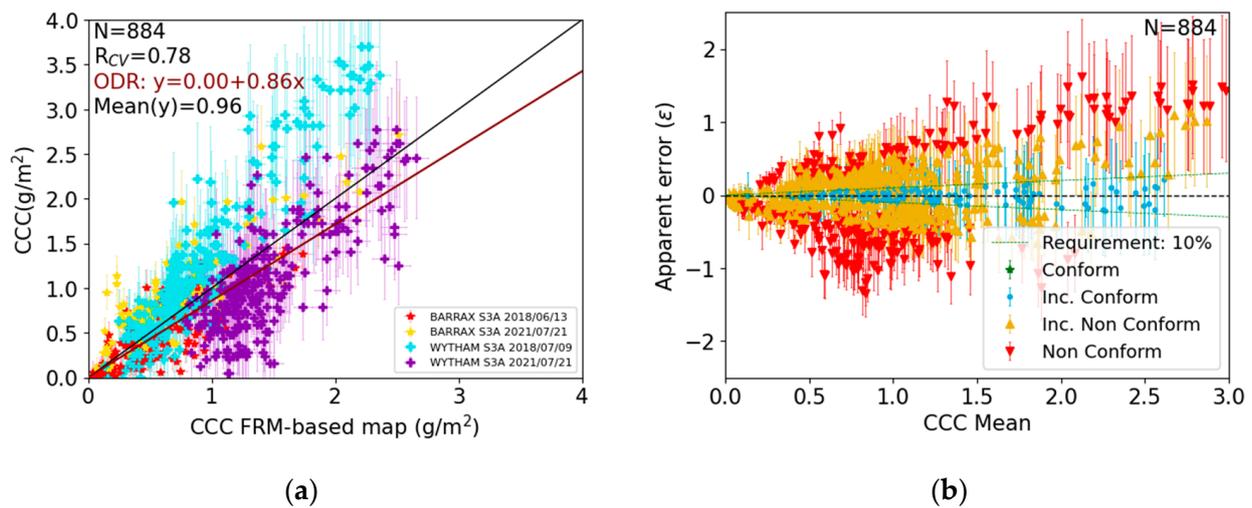

(**a**)   (**b**)

Figure A6. (**a**) Scatterplot between Sentinel-3A OTCI-based CCC and FRM-based reference maps for Las Tiesas—Barrax (crosses) and Wytham Woods (stars) sites. Vertical and horizontal bars display expanded uncertainties at coverage factor k = 2. The brown line displays the ODR fit. (**b**) Conformity testing (at k = 2) results regarding the Sentinel-3 mission requirements on accuracy. The dashed green line displays the 10% threshold requirement.

Table A2. Summary of validation metrics and conformity testing according to the Sentinel-3 mission requirements on accuracy for Sentinel-3A GIFAPAR at coverage factor k = 2.

Validation Metric		Requirement on Accuracy	Compliance (%)	
N	1070		Conclusively conforming	0.0
R	0.96	Goal (5%)	Inconclusively conforming	12.2
ODR	Y = 0.83x		Inconclusively non-conforming	78.7
B	$-0.07\,(-14.5\%)$		Conclusively non-conforming	9.1
MD	$-0.06\,(-12.2\%)$		Conclusively conforming	0.0
STD	0.09 (18.9%)	Threshold (10%)	Inconclusively conforming	29.6
MAD	0.06 (13.3%)		Inconclusively non-conforming	63.3
RMSD	0.11 (23.8%)		Conclusively non-conforming	7.1

Table A3. Summary of validation metrics and conformity testing according to the Sentinel-3 mission requirements on accuracy for Sentinel-3A OTCI-based CCC at coverage factor k = 2.

Validation Metric		Requirement on Accuracy	Compliance (%)	
N	884		Conclusively conforming	0.0
R	0.78		Inconclusively conforming	7.7
ODR	Y = 0.86x − 0.00	Goal (5%)	Inconclusively non-conforming	56.6
B	0.00 (0.2%)		Conclusively non-conforming	35.7
MD	−0.04 (−4.2%)		Conclusively conforming	0.0
STD	0.46 (47.6%)		Inconclusively conforming	16.0
MAD	0.23 (24.5%)	Threshold (10%)	Inconclusively non-conforming	53.8
RMSD	0.46 (47.6%)		Conclusively non-conforming	30.2

References

1. Balsamo, G.; Agusti-Panareda, A.; Albergel, C.; Arduini, G.; Beljaars, A.; Bidlot, J.; Bousserez, N.; Boussetta, S.; Brown, A.; Buizza, R.; et al. Satellite and In Situ Observations for Advancing Global Earth Surface Modelling: A Review. *Remote Sens.* **2018**, *10*, 2038. [CrossRef]
2. Dinguirard, M.; Slater, P.N. Calibration of Space-Multispectral Imaging Sensors: A Review. *Remote Sens. Environ.* **1999**, *68*, 194–205. [CrossRef]
3. Justice, C.; Belward, A.; Morisette, J.; Lewis, P.; Privette, J.; Baret, F. Developments in the "validation" of Satellite Sensor Products for the Study of the Land Surface. *Int. J. Remote Sens.* **2000**, *21*, 3383–3390. [CrossRef]
4. Morisette, J.T.; Baret, F.; Privette, J.L.; Myneni, R.B.; Nickeson, J.E.; Garrigues, S.; Shabanov, N.V.; Weiss, M.; Fernandes, R.A.; Leblanc, S.G.; et al. Validation of Global Moderate-Resolution LAI Products: A Framework Proposed within the CEOS Land Product Validation Subgroup. *IEEE Trans. Geosci. Remote Sens.* **2006**, *44*, 1804–1814. [CrossRef]
5. Goryl, P.; Fox, N.; Donlon, C.; Castracane, P. Fiducial Reference Measurements (FRMs): What Are They? *Remote Sens.* **2023**, *15*, 5017. [CrossRef]
6. Widlowski, J.-L. Conformity Testing of Satellite-Derived Quantitative Surface Variables. *Environ. Sci. Policy* **2015**, *51*, 149–169. [CrossRef]
7. QA4EO Documentation. Available online: https://qa4eo.org/documents/ (accessed on 6 March 2024).
8. Niro, F.; Goryl, P.; Dransfeld, S.; Boccia, V.; Gascon, F.; Adams, J.; Themann, B.; Scifoni, S.; Doxani, G. European Space Agency (ESA) Calibration/Validation Strategy for Optical Land-Imaging Satellites and Pathway towards Interoperability. *Remote Sens.* **2021**, *13*, 3003. [CrossRef]
9. Origo, N.; Gorroño, J.; Ryder, J.; Nightingale, J.; Bialek, A. Fiducial Reference Measurements for Validation of Sentinel-2 and Proba-V Surface Reflectance Products. *Remote Sens. Environ.* **2020**, *241*, 111690. [CrossRef]
10. Brown, L.A.; Camacho, F.; García-Santos, V.; Origo, N.; Fuster, B.; Morris, H.; Pastor-Guzman, J.; Sánchez-Zapero, J.; Morrone, R.; Ryder, J.; et al. Fiducial Reference Measurements for Vegetation Bio-Geophysical Variables: An End-to-End Uncertainty Evaluation Framework. *Remote Sens.* **2021**, *13*, 3194. [CrossRef]
11. Fernandes, R.; Plummer, S.; Nightingale, J.; Baret, F.; Camacho, F.; Fang, H.; Garrigues, S.; Gobron, N.; Lang, M.; Lacaze, R.; et al. Global Leaf Area Index Product Validation Good Practices. In *Best Practice for Satellite-Derived Land Product Validation*; Fernandes, R., Plummer, S., Nightingale, J., Eds.; Land Product Validation Subgroup (Committee on Earth Observation Satellites Working Group on Calibration and Validation): Greenbelt, MD, USA, 2014.
12. Nestola, E.; Sánchez-Zapero, J.; Latorre, C.; Mazzenga, F.; Matteucci, G.; Calfapietra, C.; Camacho, F. Validation of PROBA-V GEOV1 and MODIS C5 & C6 FAPAR Products in a Deciduous Beech Forest Site in Italy. *Remote Sens.* **2017**, *9*, 126. [CrossRef]
13. Camacho, F.; Cernicharo, J.; Lacaze, R.; Baret, F.; Weiss, M. GEOV1: LAI, FAPAR Essential Climate Variables and FCOVER Global Time Series Capitalizing over Existing Products. Part 2: Validation and Intercomparison with Reference Products. *Remote Sens. Environ.* **2013**, *137*, 310–329. [CrossRef]
14. Martínez, B.; Camacho, F.; Verger, A.; García-Haro, F.J.; Gilabert, M.A. Intercomparison and Quality Assessment of MERIS, MODIS and SEVIRI FAPAR Products over the Iberian Peninsula. *Int. J. Appl. Earth Obs. Geoinf.* **2012**, *21*, 463–476. [CrossRef]
15. Brown, L.A.; Meier, C.; Morris, H.; Pastor-Guzman, J.; Bai, G.; Lerebourg, C.; Gobron, N.; Lanconelli, C.; Clerici, M.; Dash, J. Evaluation of Global Leaf Area Index and Fraction of Absorbed Photosynthetically Active Radiation Products over North America Using Copernicus Ground Based Observations for Validation Data. *Remote Sens. Environ.* **2020**, *247*, 111935. [CrossRef]
16. Fuster, B.; Sánchez-Zapero, J.; Camacho, F.; García-Santos, V.; Verger, A.; Lacaze, R.; Weiss, M.; Baret, F.; Smets, B. Quality Assessment of PROBA-V LAI, FAPAR and FCOVER Collection 300 m Products of Copernicus Global Land Service. *Remote Sens.* **2020**, *12*, 1017. [CrossRef]
17. Weiss, M.; Baret, F.; Block, T.; Koetz, B.; Burini, A.; Scholze, B.; Lecharpentier, P.; Brockmann, C.; Fernandes, R.; Plummer, S.; et al. On Line Validation Exercise (OLIVE): A Web Based Service for the Validation of Medium Resolution Land Products. Application to FAPAR Products. *Remote Sens.* **2014**, *6*, 4190. [CrossRef]

18. CEOS Land Product Validation Supersites. Available online: https://lpvs.gsfc.nasa.gov/LPV_Supersites/LPVsites.html (accessed on 6 March 2024).
19. LI-COR LI-COR Inc. 2200C_Manual_14112.Pdf|Con La Tecnología de Box. 2013. Available online: https://licor.app.box.com/s/fqjn5mlu8c1a7zir5qel (accessed on 9 February 2024).
20. ACCUPAR LP-80—METER Group. Available online: https://metergroup.com/products/accupar-lp-80/ (accessed on 6 March 2024).
21. Weiss, M.; Baret, F. *CAN_EYE V6.4.91 User Manual to Cite This Version: HAL Id: Hal-02788819*; INRA EMMA: Avignon, France, 2021.
22. Li, W.; Fang, H.; Wei, S.; Weiss, M.; Baret, F. Critical Analysis of Methods to Estimate the Fraction of Absorbed or Intercepted Photosynthetically Active Radiation from Ground Measurements: Application to Rice Crops. *Agric. For. Meteorol.* **2021**, *297*, 108273. [CrossRef]
23. Gobron, N.; Pinty, B.; Aussedat, O.; Chen, J.M.; Cohen, W.B.; Fensholt, R.; Gond, V.; Huemmrich, K.F.; Lavergne, T.; Mélin, F.; et al. Evaluation of Fraction of Absorbed Photosynthetically Active Radiation Products for Different Canopy Radiation Transfer Regimes: Methodology and Results Using Joint Research Center Products Derived from SeaWiFS against Ground-Based Estimations. *J. Geophys. Res.* **2006**, *111*, D13110. [CrossRef]
24. Minolta. *Chlorophyll Meter SPAD-502*; Minolta: Osaka, Japan, 2009; pp. 1–22.
25. Brown, L.A.; Williams, O.; Dash, J. Calibration and Characterisation of Four Chlorophyll Meters and Transmittance Spectroscopy for Non-Destructive Estimation of Forest Leaf Chlorophyll Concentration. *Agric. For. Meteorol.* **2022**, *323*, 109059. [CrossRef]
26. DLR. *AGRISAR 2006—Agriculural Bio-/Geophysical Retrievals from Frequent Repeat SAR and Optical Imaging: Data Aquisition Report*; Deutsches Zentrum für Luft- und Raumfahrt: Oberpfaffenhofen, Germany, 2006.
27. Gorroño, J.; Fomferra, N.; Peters, M.; Gascon, F.; Underwood, C.; Fox, N.; Kirches, G.; Brockmann, C. A Radiometric Uncertainty Tool for the Sentinel 2 Mission. *Remote Sens.* **2017**, *9*, 178. [CrossRef]
28. Gorroño, J.; Hunt, S.; Scanlon, T.; Banks, A.; Fox, N.; Woolliams, E.; Underwood, C.; Gascon, F.; Peters, M.; Fomferra, N.; et al. Providing Uncertainty Estimates of the Sentinel-2 Top-of-Atmosphere Measurements for Radiometric Validation Activities. *Eur. J. Remote Sens.* **2018**, *51*, 650–666. [CrossRef]
29. Martínez, B.; García-Haro, F.J.; Camacho, F. Derivation of High-Resolution Leaf Area Index Maps in Support of Validation Activities: Application to the Cropland Barrax Site. *Agric. For. Meteorol.* **2009**, *149*, 130–145. [CrossRef]
30. Donlon, C.; Berruti, B.; Buongiorno, A.; Ferreira, M.H.; Féménias, P.; Frerick, J.; Goryl, P.; Klein, U.; Laur, H.; Mavrocordatos, C.; et al. The Global Monitoring for Environment and Security (GMES) Sentinel-3 Mission. *Remote Sens. Environ.* **2012**, *120*, 37–57. [CrossRef]
31. Gobron, N.; Pinty, B.; Verstraete, M.M.; Widlowski, J.-L. Advanced Vegetation Indices Optimized for Up-Coming Sensors: Design, Performance, and Applications. *IEEE Trans. Geosci. Remote Sens.* **2000**, *38*, 2489–2505. [CrossRef]
32. Rahman, H.; Pinty, B.; Verstraete, M.M. Coupled Surface-Atmosphere Reflectance (CSAR) Model: 2. Semiempirical Surface Model Usable with NOAA Advanced Very High Resolution Radiometer Data. *J. Geophys. Res.* **1993**, *98*, 20791. [CrossRef]
33. Gobron, N. *Ocean and Land Colour Instrument (OLCI) FAPAR and Rectified Channels over Terrestrial Surfaces Algorithm Theoretical Basis Document*; European Commission Joint Research Centre: Ispra, Italy, 2010.
34. Horler, D.N.H.; Dockray, M.; Barber, J. The Red Edge of Plant Leaf Reflectance. *Int. J. Remote Sens.* **1983**, *4*, 273–288. [CrossRef]
35. Dash, J.; Curran, P.J. The MERIS Terrestrial Chlorophyll Index. *Int. J. Remote Sens.* **2004**, *25*, 5403–5413. [CrossRef]
36. Dash, J. *Algorithm Theoretical Basis Document: OLCI Terrestrial Chlorophyll Index (OTCI)*; University of Southampton: Southampton, UK, 2012.
37. *JCGM-VIM International Vocabulary of Metrology-Basic and General Concepts and Associated Terms (VIM) 3rd Edition 2008 Version with Minor Corrections*; International Organization of Legal Metrology (IOLM): Paris, France, 2012.
38. Drinkwater, M.; Rebhan, H. *Sentinel-3: Mission Requirements Document*; European Space Agency: Noordwijk, The Netherlands, 2007.
39. *ISO 10576:2022*; Statistical Methods—Guidelines for the Evaluation of Conformity with Specified Requirements. ISO: Geneva, Switzerland, 2022. Available online: https://www.iso.org/es/contents/data/standard/07/88/78878.html?browse=ics (accessed on 6 June 2024).
40. Mira, M.; Weiss, M.; Baret, F.; Courault, D.; Hagolle, O.; Gallego-Elvira, B.; Olioso, A. The MODIS (Collection V006) BRDF/Albedo Product MCD43D: Temporal Course Evaluated over Agricultural Landscape. *Remote Sens. Environ.* **2015**, *170*, 216–228. [CrossRef]
41. Weiss, M.; Baret, F.; Garrigues, S.; Lacaze, R. LAI and FAPAR CYCLOPES Global Products Derived from VEGETATION. Part 2: Validation and Comparison with MODIS Collection 4 Products. *Remote Sens. Environ.* **2007**, *110*, 317–331. [CrossRef]
42. Li, W.; Baret, F.; Weiss, M.; Buis, S.; Lacaze, R.; Demarez, V.; Dejoux, J.-F.; Battude, M.; Camacho, F. Combining Hectometric and Decametric Satellite Observations to Provide near Real Time Decametric FAPAR Product. *Remote Sens. Environ.* **2017**, *200*, 250–262. [CrossRef]
43. Gobron, N.; Morgan, O.; Adams, J.; Brown, L.A.; Cappucci, F.; Dash, J.; Lanconelli, C.; Marioni, M.; Robustelli, M. Evaluation of Sentinel-3A and Sentinel-3B Ocean Land Colour Instrument Green Instantaneous Fraction of Absorbed Photosynthetically Active Radiation. *Remote Sens. Environ.* **2022**, *270*, 34–4257. [CrossRef]
44. Wojnowski, W.; Wei, S.; Li, W.; Yin, T.; Li, X.X.; Ow, G.L.F.; Yusof, M.L.M.; Whittle, A.J. Comparison of Absorbed and Intercepted Fractions of PAR for Individual Trees Based on Radiative Transfer Model Simulations. *Remote Sens.* **2021**, *13*, 1069. [CrossRef]
45. Origo, N.J. Measuring and Modelling FAPAR for Satellite Product Validation. Ph.D. Thesis, UCL, London, UK, 2023.

46. Brown, L.A.; Morris, H.; Morrone, R.; Sinclair, M.; Williams, O.; Hunt, M.; Bandopadhyay, S.; Guo, X.; Akcay, H.; Dash, J. Near-Infrared Digital Hemispherical Photography Enables Correction of Plant Area Index for Woody Material during Leaf-on Conditions. *Ecol. Inform.* **2024**, *79*, 102441. [CrossRef]

47. The 2022 GCOS ECVs Requirements (GCOS 245) | E-Library. Available online: https://library.wmo.int/index.php?lvl=notice_display&id=22135#.ZGI07nZBxPZ (accessed on 15 May 2023).

48. Garrigues, S.; Lacaze, R.; Baret, F.; Morisette, J.T.; Weiss, M.; Nickeson, J.E.; Fernandes, R.; Plummer, S.; Shabanov, N.V.; Myneni, R.B.; et al. Validation and Intercomparison of Global Leaf Area Index Products Derived from Remote Sensing Data. *J. Geophys. Res. Biogeosci.* **2008**, *113*, G02028. [CrossRef]

49. Fang, H.; Baret, F.; Plummer, S.; Schaepman-Strub, G. An Overview of Global Leaf Area Index (LAI): Methods, Products, Validation, and Applications. *Rev. Geophys.* **2019**, *57*, 739–799. [CrossRef]

50. Brown, L.A.; Ogutu, B.O.; Camacho, F.; Fuster, B.; Dash, J. Deriving Leaf Area Index Reference Maps Using Temporally Continuous in Situ Data: A Comparison of Upscaling Approaches. *IEEE J. Sel. Top. Appl. Earth Obs. Remote Sens.* **2021**, *14*, 624–630. [CrossRef]

51. Camacho, F.; Martinez-Sanchez, E.; Sanchez-Zapero, J.; Dash, J.; Brown, L.A.; Origo, N.; Morris, H.; Morrone, R.; Morven, S. Is the CEOS LPV 2-Stage Validation Approach Suitable for Conformity Testing of Moderate Resolution Satellite Products?: Outcomes of the FRM4Veg Project. In Proceedings of the European Space Agency Workshop on Land Product Validation and Evolution, Frascati, Italy, 12–14 June 2023.